A wave-to-wire analysis of the adjustable draft point absorber wave energy converter coupled with a linear permanent-magnet generator

Tan, Jian; Polinder, Henk; Laguna, Antonio Jarquin; Miedema, Sape

Important note
To cite this publication, please use the final published version (if applicable).
Please check the document version above.

A wave-to-wire analysis of the adjustable draft point absorber wave energy converter coupled with a linear permanent-magnet generator

Jian Tan [*], Henk Polinder, Antonio Jarquin Laguna, Sape Miedema

Department of Maritime & Transport Technology, Delft University of Technology, The Netherlands

ARTICLE INFO

ABSTRACT

An adjustable draft point absorber was recently proposed as a novel approach to improve power absorption with constrained power take-off (PTO) capacities. The key feature of the novel wave energy converter (WEC) concept is to adjust the buoy draft by regulating the ballast water inside the buoy, which aims to enable variation of the natural frequency of the WEC. Although previous research has shown benefits for the energy absorption stage, the impact of the draft adjustment on the power conversion efficiency and overall performance has not been examined yet. Therefore, a wave-to-wire model is established to provide an in-depth insight into the systematic performance of the adjustable draft point absorber integrated with a linear permanent magnet generator. Both a nonlinear hydrodynamic model and an analytical generator model are derived, thus the complete process from the wave power input through the whole WEC system to the usable electricity is covered. Based on the established model, wave-to-wire responses of the novel concept are obtained and analyzed. The negative effects of the draft adjustment on the stroke and overlap between the stator and translator are demonstrated. Moreover, a comparison is made between this novel WEC and conventional fixed draft WEC, and both regular and irregular wave states are considered. The results show that the adjustable draft system could increase not only the absorbed power but also the generator conversion efficiency. In specific conditions, the delivered electrical power of the adjustable draft WEC was over 20 % and 10 % higher than a traditional fixed draft system for regular and irregular waves respectively.

1. Introduction

Ocean waves carry a considerable amount of clean energy, which can be expected to play a role in the worldwide energy transition. The exploitation of wave energy has been receiving significant research interest over the last decades (Falcão, 2010). A number of concepts of wave energy converters (WECs) have been proposed and even tested (Aderinto and Li, 2018; Lehmann et al., 2017). However, as indicated in De Andres et al. (2017), the economic performance of WECs is far from being satisfying. The levelized cost of energy (LCOE) of WECs is estimated to be clearly higher than other competitive technologies of renewable energy. This is regarded as a big hurdle on the path toward the large-scale utilization of WECs (Clemente et al., 2021; Roberts et al., 2016).

The sizing of power take-off (PTO) systems has been proven to be of importance to the economic performance of WECs (Tan et al., 2021a, 2022b; Tokat, 2018). As a core component, PTO systems are in charge of converting the absorbed power to usable electricity. During operation, the PTO capacity is associated with physical constraints,

such as the peak power and force limit. From this perspective, increasing the PTO capacity could contribute to the improvement of total power production. However, the PTO system applied in wave energy conversion is an expensive component, and its cost normally accounts for more than 20% of the total capital expenditures (CAPEX) (Tokat, 2018). Enlarging the PTO capacity would lead to an obvious increase in the CAPEX. Therefore, it is essential to make a compromise between the power production and the cost during the sizing of the PTO capacity. The influence of the PTO sizing on the LCOE was studied in Tan et al. (2021a), and three realistic wave sites were considered. The results showed that the PTO sizing is influential to the techno-economic performance, and suitably downsizing the PTO capacity would penalize the annual energy production (AEP) but reduce the LCOE.

The downsized PTO capacity inevitably leads to stricter force and power limitations. These limitations are more relevant in powerful wave states, and therefore it is to the disadvantage of the power absorption. Solutions to improving the power performance of WECs subjected to constraints of PTO capacities have been explored, which are discussed below.

- The first type of method concentrates on the aspect of PTO control strategies. Elisabetta Tedeschi and Marta Molinas (Tai et al., 2012; Tedeschi and Molinas, 2010, 2012; Tedeschi et al., 2011) investigated the impacts of control strategies on the PTO rating of WECs. A generic point absorber was used as the research object. It was found that the reactive control strategy clearly improves power absorption but requires higher PTO capacities. In contrast, the passive control strategy could reduce the required PTO capacities while it corresponds to low power absorption. In order to reach a suitable PTO rating and retain an adequate level of power production at the same time, they came up with a trade-off tactic by adapting the PTO control strategy to different wave states.

- The second type of method is to increase the speed of the buoy by means of adding an intermediate transmission mechanism, such as a gearbox. For instance, a linear generator coupled with a speed amplifying gearbox was designed for a WEC concept in Liu et al. (2021), in which the relative speed between the stator and translator was therefore increased. In this sense, a smaller PTO force is sufficient to supply a similar output power level with low-speed PTO systems. However, the addition of transmission stages in the PTO system could decrease the reliability and conversion efficiency.

- Alternatively, an adjustable draft system has been recently proposed to improve the power performance of point absorbers operating in conditions with constrained PTO forces (Tan et al., 2020). The system was designed to implement the buoy draft adjustment by changing the ballast water inside the buoy. In this way, both the hydrostatic stiffness and mass of the buoy can be regulated, which enables the variation of the buoy's natural frequency. Subsequently, increased displacement and speed can be achieved over a range of wave periods for the buoy. As a consequence, the power absorption of WECs coupled with the adjustable draft system tends to be less affected by the downsized PTO capacity with regard to the conventional fixed-draft point absorbers.

The draft adjustment in the proposed adjustable draft system is realized by changing the ballast water inside the buoy. In recent years, the influence of the ballast and draft design on the performance of WECs has been analyzed in a few of the literature, in which its importance was emphasized. In Flocard and Finnigan (2012) and Qiu et al. (2013) the effect of ballast configuration on the power absorption efficiency was analyzed by experimental studies. According to their results, the power capture factor can be increased by 15% to 40% in irregular wave states. In Colby et al. (2011), an optimization of the ballast geometry of a floating wave energy converter was carried out using an evolutionary algorithm. The optimized ballast design leads to an 84% improvement in power production compared to the ballast-free device. In Wang and Ringwood (2021), the ballast design of a three-body hinge-barge type wave energy converter was analyzed, in which the influence of control strategy and geometrical size were taken into consideration. It showed that the center of gravity of the device is strongly related to the ballast configuration, which has a significant influence on the power performance of that type of WEC. In a particular irregular sea state, the maximum improvement in the power output resulting from the optimized ballast design reaches 70.8% over the original configuration. In Temiz et al. (2021), the influence of ballast distribution on the initial rest angle, the moment of inertia, RAO (response amplitude operator) and power production of a pitching WEC was studied. To save the computational load, an analytical model was formulated to accelerate the ballast optimization. The results indicated that increasing the ballast inertial moment leads to lower resonance frequencies and higher peak responses. Besides, it suggested that the ballast design could make a remarkable impact on the power absorption in sea states with a peak period below the range of attainable resonance

periods of the pitching absorber. The impact of the draft design on the hydrodynamic performance of a floating WEC was studied in Stallard et al. (2009) by means of experimental tests. The results showed that the heaving responses in heavy waves can be effectively limited by varying the draft to cause upper surface immersion of the floater. In Wang et al. (2022a) and Wang et al. (2022e), a control-strategy-informed optimization routine was established and applied to search for the optimal geometry for WECs, in which the buoy draft or water ballast positioning was considered as one of the optimization variables. The results showed that the buoy draft or the water ballast could make a clear difference in energy harvesting. It is noted that the literature mentioned above mainly focused on the relevance of the ballast or draft on the hydrodynamic performance and power absorption stage of WECs, while the adjustable draft system was designed with an emphasis on mitigating the negative effects of downsizing PTO capacities.

The conceptual design of the adjustable draft WEC has been proven to be of much potential in Tan et al. (2020) and Tan et al. (2022a), but the effects of the draft adjustment on the systematic performance of the WEC still remain unclear. Specifically, applying the adjustable draft system is able to increase the absorbed power for point absorbers with downsized PTO systems. However, as a whole system, the draft variation would inevitably make a difference to the PTO performance. On the one hand, the adjustable draft system contributes to a higher buoy velocity. In electrical generators, the higher translator velocity is normally associated with fewer copper losses and then higher conversion efficiency. On the other hand, as the buoy of point absorbers is commonly coupled with the PTO system, the draft variation could affect the symmetry of the effective stroke. Particularly, if the linear generator is used as the PTO system, the draft variation could also have an influence on the duration of the partial overlap between the translator and stator. As presented in Tan et al. (2022b), during the partial overlap only a portion of the stator is used and the stator current has to be driven higher for supplying the required PTO force, which thus implies the reduction of the efficiency of the generator. Nevertheless, these effects on the PTO system and the overall performance of the WEC were not discussed in Tan et al. (2022a). Instead, it was only investigated in such a way assuming a simplified damper-like PTO model. To provide a solid performance evaluation of the WEC applying the adjustable draft system, it is of significance to carry out a wave-to-wire analysis on all the relevant energy conversion stages of the WEC, including the wave-buoy hydrodynamics, energy transmission, and electricity generation.

A variety of wave-to-wire models have been developed in the recent years. Regarding the power absorption stage, the wave-buoy hydrodynamics can be calculated by linear modeling, weakly nonlinear modeling or fully nonlinear modeling. From the perspective of energy transmission, wave-to-wire models differ by using pneumatic, hydraulic or mechanical PTO modeling. For the electricity generation stage, wave-to-wire models could be mainly divided by applying the rotary or linear electric generator model. For instance, a high-fidelity wave-to-wire model was proposed and validated for point absorbers in Penalba and Ringwood (2019), Penalba et al. (2017d) and Penalba et al. (2017a). The nonlinear Froude–Krylov force and viscous force were incorporated into the hydrodynamic model, and a hydraulic PTO model coupled with a rotary electric generator model was used to mimic the power transmission and generation stages. By means of the proposed model, the influence of the configuration of the hydraulic PTO system on systematic performance was investigated. In Forehand et al. (2015), a wave-to-wire model was presented for studying an array of point absorbers. It was established by integrating a hydrodynamic model including the nonlinear hydrostatic force, a hydraulic PTO model, an induction rotary generator model and an electric network model. The interaction between the electric network and the dynamic responses of the array was studied, and the importance of the wave-to-wire model in the whole system design was identified. A fully-coupled model was applied in Saenz-Aguirre et al. (2021) to demonstrate the

power improvement of the point absorbers with a linear generator by using a field weakening control strategy in the PTO system. A linear hydrodynamic model and an electric model of linear generators are included in the wave-to-wire model, and the power production of the WECs at various wave states was revealed. In recent years, authors in Wang et al. (2020), Wang (2017) and Wang et al. (2022c) have carried out a series of wave-to-wire studies for point absorbers with linear PM generators. It has been indicated in Wang et al. (2020) and Wang et al. (2022c) that, for an isolated WEC connected to a DC circuit, the tuning of electric loads could play a significant role in electrical power generation. An optimization routine was proposed in their studies to obtain the optimal resistor value for improving the electrical power. In Josset et al. (2007), the wave-to-wire model was derived for a pendulum-type WEC with a PTO system comprising hydraulic rams, an accumulator and a hydraulic generator. The model results showed that electricity production can be discontinuous in irregular wave states. This is because the converted power by the considered electrical generator was at a higher rate than the power transmitted from the hydraulic rams to the accumulator. The wave-to-wire process of oscillating water column (OWC) devices has also been studied in a set of recent literature (Ciappi et al., 2020, 2022a,b; Suchithra et al., 2019; Gurnari et al., 2020; Benreguig et al., 2019; Kelly et al., 2015; Bailey et al., 2016; Liu et al., 2022). These studies applied different methods to model the hydrodynamics, aerodynamics and thermodynamics of the air chamber and air turbines. The interaction between the air turbines and the electrical generators was also analyzed. Various air chamber designs coupled with Wells turbines or impulse turbines were considered in the studies, and their power performance was identified.

As a follow-up study of Tan et al. (2022a), the objective of the present paper is to establish a wave-to-wire model for the adjustable draft WEC and thoroughly reveal the impacts of the adjustable draft system on power performance. The paper starts with a brief description of the adjustable draft WEC. Next, the formulation of the wave-to-wire model is presented. An algebraic nonlinear time domain model is applied to simulate the dynamic behavior of the WEC, in which two nonlinear force components, namely the nonlinear Froude–Krylov force and viscous force, are included. The responses of the linear generator are calculated by an analytical model, in which the no-load voltage, current, losses and resulting generator force can be obtained. The negative effects resulting from the draft adjustment on the power performance are studied, including the non-symmetry of the stroke and the partial overlap between the stator and translator. The delivered electrical power and PTO conversion efficiency of the WEC are identified in both regular and irregular wave conditions. A performance comparison between the adjustable draft absorber and the semi-submerged fixed draft point absorber is made. Finally, a conclusion is drawn.

2. Concept description

This section describes the conceptual design of the adjustable draft WEC. A generic heaving point absorber is used as the WEC reference in this study. During the operation, the floating buoy of the point absorber is excited by incoming waves to move up and down, in which wave power is captured by the buoy as mechanical energy. Then, the mechanical energy stored in the motion of the buoy is taken by the PTO system and converted to usable electricity. The geometry of the floating buoy is a sphere with a radius of 3.5 m. The schematic of the adjustable draft WEC concept is shown in Fig. 1(a). In the adjustable draft WEC concept, a ballast pump is installed for implementing the adjustment of the buoy draft. The adjustable range of the buoy draft, indicated by h_a in Fig. 1(a), is defined as from 3.5 m to 5.0 m in the present study, although the desired range could differ with the variation of buoy geometry, size and wave resource. The total mass of the buoy can be changed by varying the ballast water inside the buoy. It is assumed that the buoy without ballast water naturally floats at the minimum draft of 3.5 m in still water. The ballast water inside the buoy is regulated

by the pump to reach a certain buoy draft. It is assumed that the draft could be efficiently adjusted to the expected value in each wave state. A linear generator is bottom-founded serving as the PTO system, and the translator is directly connected to the buoy. A back-to-back electronic converter is equipped after the generator to connect the WEC to the electrical grid (Polinder et al., 2004) (see Fig. 1).

As the allowable stroke is unchangeable for a certain linear generator, increasing the buoy draft reduces the lower half of the stroke. For a compromise, the translator is therefore placed at the position where the horizontal center lines of the translator and stator are aligned when the buoy draft is 4.25 m. The effects of the draft adjustment on the motion of the buoy and the overlap between the stator and translator are demonstrated in detail in Section 4.3. In addition, the displacement of the buoy is limited to protect the structure, and the limit is set to 0.8 times the radius of the spherical buoy in this work.

3. Wave-to-wire modeling

The wave-to-wire model established in this paper comprises three main components: representation of wave input, nonlinear hydrodynamic modeling and analytical generator modeling. The diagram of the model is shown in Fig. 2. The incoming waves are considered unidirectional Airy waves. Nonlinear time-domain hydrodynamic modeling is adopted to describe the wave-buoy interaction. An analytical generator model is used to mimic the responses of the linear generator and converter. The hydrodynamic and electrical models are linked in such a way that the position and velocity of the buoy are taken as inputs to the generator and the generator makes the corresponding PTO force interact with the dynamics of the buoy. The simulation is performed based on the numerical integration scheme ODE solver in MATLAB environment. The main formulations of each stage in the wave-to-wire model are presented in the following text.

3.1. Stage 1: Representation of incoming waves

The incoming waves are represented based on linear wave theory, and unidirectional waves are considered in this work (Falnes, 2003). The regular wave input is defined as

$$\eta_{re}(t) = \zeta_a \cos(kx - \omega t) \tag{1}$$

where t is time, k is the wave number, ω is the angular frequency of the incoming wave and ζ_a is the wave amplitude. Based on the superposition theory, irregular waves are expressed as

$$\eta_{irr}(t) = \sum_{j=1}^{N} \zeta_a(\omega_j) \cos(k(\omega_j)x - \omega_j t + \varphi(\omega_j)) \tag{2}$$

where η_{irr} is the wave elevation in irregular wave states, j corresponds to the j_{th} frequency component, and N is the total number of the considered frequency components; $k(\omega_j)$, $\zeta_a(\omega_j)$ and $\varphi_{(\omega_j)}$ are the wave number, wave amplitude and phase of the regular wave component corresponding to wave frequency ω_j. The Jonswap spectrum with a peakedness factor of 3.3 is applied in this work, but the expression (2) is also flexible to other wave spectra (Journée et al., 2015).

3.2. Stage 2: Nonlinear hydrodynamic modeling

The interaction between the buoy and incoming waves is described by hydrodynamic modeling. The buoy is constrained to move in a heaving direction, and only this degree of freedom is discussed. The motion of a floating buoy can be described based on Cummins equation (Cummins et al., 1962) as

$$(m + M_r(\infty))\ddot{z}(t) = F_{FK_{st}} - mg + F_{FK_{dy}} + F_{ge} + F_D + F_{vis}$$
$$+ \int_{-\infty}^{t} K_{rad}(t - \tau)\dot{z}(\tau)d\tau \tag{3}$$
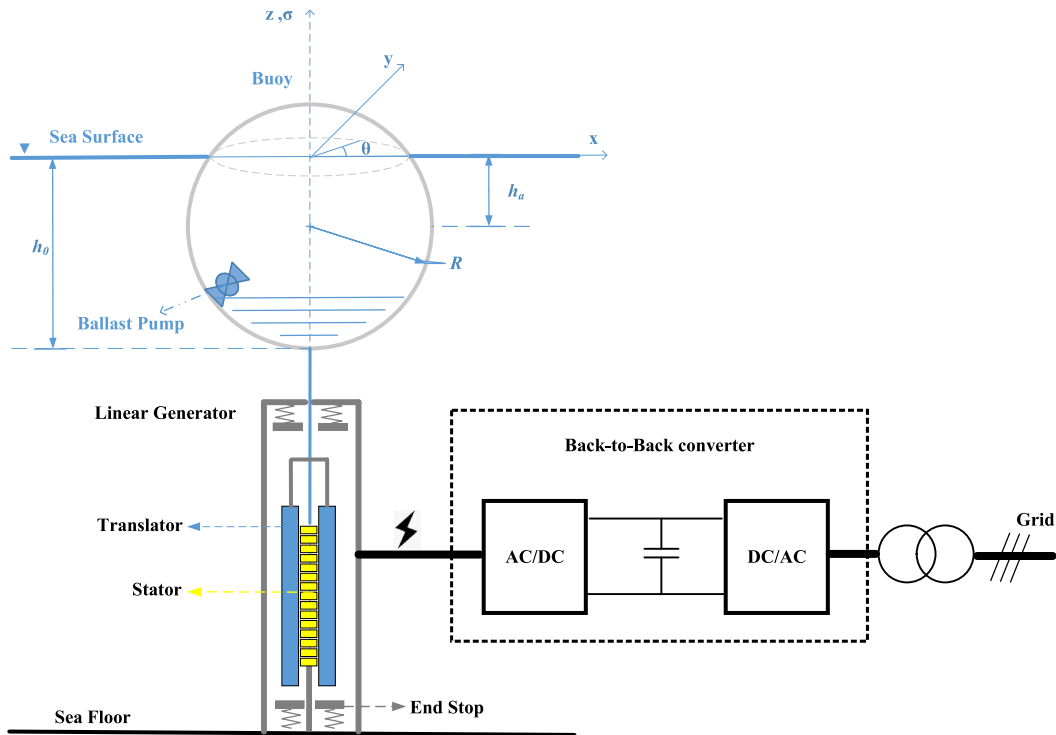
(a) Schematic of the adjustable draft point absorber with a linear PM generator connected to the grid via a back-to-back converter
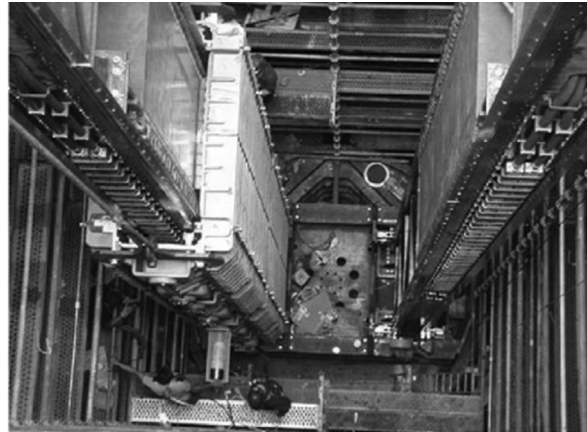
(b) On-site photo of the linear PM machine applied in AWS WEC [43]

Fig. 1. Illustration of the concept of the adjustable draft WEC studied in this work.

in which m is the mass of the oscillating body, $F_{FK_{st}}$ is the static Froude–Krylov force, $F_{FK_{dy}}$ is the dynamic Froude–Krylov force, F_D is the diffraction force, K_{rad} radiation impulse function, F_{ge} is the PTO force or generator force, z is the displacement of the buoy, $\dot{z}$ is the velocity of the buoy, F_{vis} is the viscous force, and F_{es} is the end stop force for preventing the excessive displacement of the buoy. $M_r(\infty)$ and K_{rad} represent the added mass evaluated at the infinite frequency and the radiation impulse function. They are calculated based on the results of hydrodynamic damping $R_i(\omega)$ and added mass $M_r(\omega)$.

The Froude–Krylov force components, including $F_{FK_{st}}$ and $F_{FK_{dy}}$, are defined as the integration of incoming wave pressure over the wetted surface of the body. The nonlinear Froude–Krylov forces are calculated by an algebraic method (Giorgi and Ringwood, 2017a,d). In the method, the pressure is derived based on linear wave theory, but the instantaneous wetted surface and free surface are considered. As stated in Tan et al. (2022a), for spherical buoys with arbitrary drafts, the algebraic solutions to nonlinear Froude–Krylov forces can be obtained

as

$$F_{FK_{st}} = -2\pi\rho g \left[\frac{\sigma^3}{3} + (z(t) - h_0 + R)\frac{\sigma^2}{2} \right]_{\sigma_1}^{\sigma_2} \tag{4}$$

$$F_{FK_{dy(re)}} = -\frac{2\pi}{k}\rho g a \cos(-\omega t) \left[((z(t) - h_0 + R) + \frac{1}{k} - \sigma)e^{k\sigma} \right]_{\sigma_1}^{\sigma_2} \tag{5}$$

in which $F_{FK_{st}}$ represents the static Froude–Krylov force, $F_{FK_{dy(re)}}$ represents the dynamic Froude–Krylov force in regular wave conditions, k is the wave number, ρ stands for the water density, σ is the vertical coordinate in the parametric cylindrical coordinate system, z is the vertical displacement of the buoy, h_0 is the draft of the buoy in still water, and R is the radius of the spherical buoy. The integral limits, namely σ_1 and σ_2, are defined as

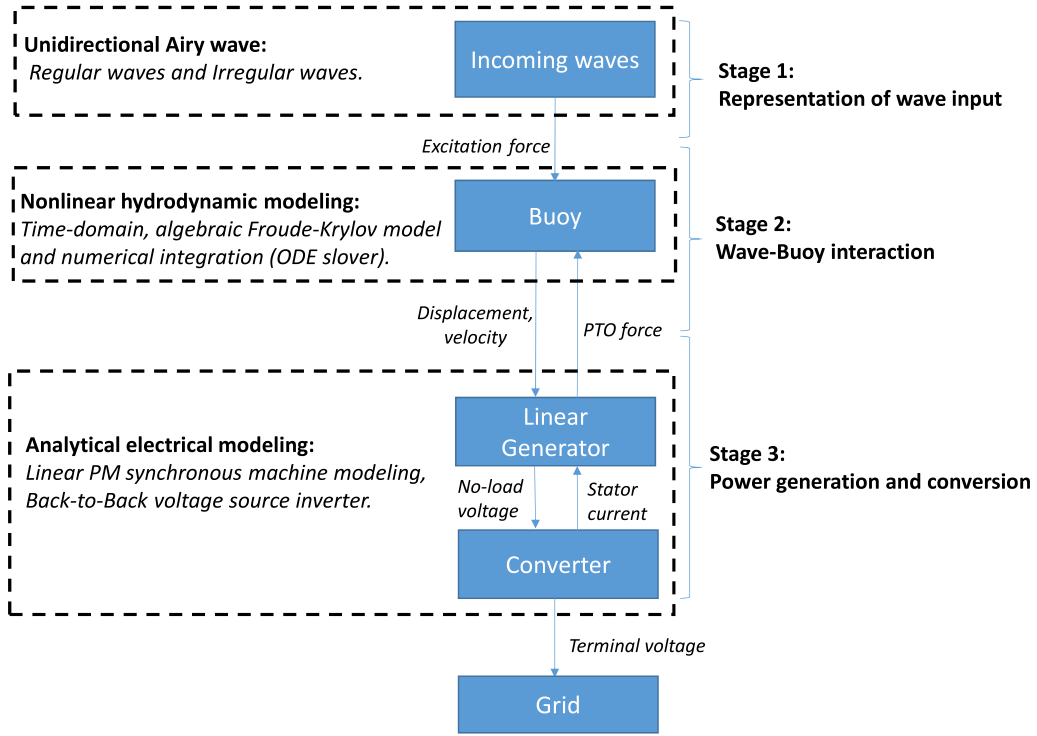$$\begin{cases} \sigma_1 = z(t) - h_0 \\ \sigma_2 = \eta(t) \end{cases} \tag{6}$$

Fig. 2. Diagram of the established wave-to-wire model.

where η represents instantaneous wave elevation. In irregular waves, the solution to the dynamic Froude–Krylov force is adapted to be (7) based on the superposition theory (Tan et al., 2022a), while other formulations remain identical.

$$F_{FK_{dy(irr)}} = \sum_{j=1}^{N} -\frac{2\pi}{k(\omega_j)} \rho g \zeta_a(\omega_j)(\cos(-\omega_j t + \varphi(\omega_j))) \\ \left[((z(t) - h_0 + R) + \frac{1}{k(\omega_j)} - \sigma)e^{k(\omega_j)\sigma} \right]_{\sigma_1}^{\sigma_2} \tag{7}$$

where $F_{FK_{dy(irr)}}$ embodies the dynamic Froude–Krylov force in irregular wave conditions. During the calculation of the nonlinear Froude–Krylov force, Wheeler stretching theory is used to modify the pressure profile in order for a better modeling accuracy (Giorgi and Ringwood, 2017c).

As the passive control strategy is used for the WEC in this paper, the PTO force can be expressed as

$$F_{ge}(t) = -B_{pto}\dot{z}(t) \tag{8}$$

where F_{ge} represents the generator force, and B_{pto} represents the PTO damping coefficient. The variation of PTO damping implies the control of the PTO force acting on the WEC. This is realized by the back-to-back voltage source electronic inverter to regulate the stator current and terminal voltage (Polinder et al., 2004). The operation of the inverter will be detailed in the next subsection. According to Giorgi and Ringwood (2017a), the diffraction force is calculated as

$$F_D(t) = -\int_{-\infty}^{\infty} K_{diff}(t - \tau)\eta(\tau)\mathrm{d}\tau \tag{9}$$

where K_{diff} is the diffraction impulse function, τ is an intermediate variable.

An end-stop force is applied to prevent the buoy from exceeding the predefined displacement limit, and it can be expressed as

$$F_{es}(t) = \begin{cases} 0, & |z(t)| \leq S_m \\ -K_{es}\frac{z(t)-S_m}{|z(t)-S_m|}|z(t) - S_m|, & |z(t)| > S_m \end{cases} \tag{10}$$

where F_{es} represents the end-stop force, K_{es} is the stiffness coefficient of the end-stop spring, and it is set as 500 kN/m in this work; z is

the magnitude of the vertical displacement and S_m is the displacement limit.

The viscous drag force can be calculated as such a term similar to the drag component in Morison's equation (Babarit et al., 2012), as

$$F_{vis} = -\frac{1}{2}\rho C_D A_D |\dot{z} - u_0|(\dot{z} - u_0) \tag{11}$$

where F_{vis} is the viscous force, ρ is water density, C_D is the drag coefficient, A_D is the characteristic area of the buoy, and u_0 embodies the undisturbed flow velocity at the centroid of the buoy. Given the buoy geometry, a value of 0.6 is selected as the drag coefficient A_D, referring to Giorgi and Ringwood (2017b).

3.3. Stage 3: Analytical electrical modeling

The linear generator and the electronic converter are in charge of converting mechanical energy to usable electricity, and this process is described by analytical electrical modeling. During operation, the incoming waves excite the motion of the buoy which is connected to the translator of the generator, and thus the no-load voltage is induced. Correspondingly, the generator produces the resulting PTO force to interact with the dynamics of the buoy. The main formulations of the applied electrical modeling are presented as follows.

According to Polinder et al. (2004), the fundamental space harmonic of the magnetic flux density in the air gap resulting from the magnets can be calculated as

$$\hat{B}_{gm} = \frac{l_m}{\mu_{rm}g_{eff}}B_{rm}\frac{4}{\pi}\sin(\frac{\pi b_p}{2\tau_p}) \tag{12}$$

where $\hat{B}_{gm}$ is the fundamental space harmonic of the magnetic flux density in the air gap, l_m is the magnet length in the magnetization direction, g_{eff} is the effective air gap, μ_{rm} is the recoil permeability of the magnets, B_{rm} is the remanent flux density of the magnets, b_p is the magnet pole width, and τ_p is the pole pitch. Then, the root mean square (RMS) of the no-load phase voltage induced by this flux density in the stator winding is

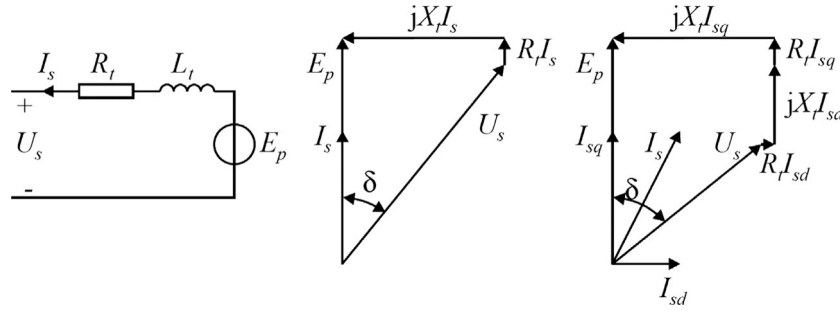$$E_p = \sqrt{2}|\dot{z}|p l_s N_s k_w \hat{B}_{gm}\frac{l_{act}}{L_{sta}} \tag{13}$$

Fig. 3. Equivalent circuit of the linear PM generator and the phasor diagram with the converter. R_t and X_t embody the stator phase resistance and stator phase reactance.

where E_p is the no-load voltage, p is the number of pole pairs, l_s is the stack length, N_s is the number of conductors per slot, l_{act} is the actual length of the overlap between the stator and translator, L_{sta} is the stator length, and k_w is the winding factor.

The iron losses are dependent on the generator frequency, which can be calculated as

$$P_{Fes} = P_{Fe0} \left(m_{Fest} \left(\frac{\hat{B}_{st}}{B_0} \right)^2 + m_{Fesy} \left(\frac{\hat{B}_{sy}}{B_0} \right)^2 \right) \frac{f_e}{f_0} \frac{l_{act}}{L_{sta}} \tag{14}$$

where P_{Fe} is the total iron losses of the generator, P_{Fe0} is the iron loss per unit mass at the frequency f_0 and flux density B_0; m_{Fest} and m_{Fesy} are the mass of the stator teeth and the stator yoke respectively; f_e is the electrical generator frequency which is dependent on the buoy velocity, and $\hat{B}_{st}$ and $\hat{B}_{sy}$ embody the fundamental space harmonic of magnetic flux density in the stator teeth and yoke. $\hat{B}_{st}$ and $\hat{B}_{sy}$ can be calculated as

$$\hat{B}_{st} = \hat{B}_{gm} \frac{\tau_s}{b_t} \tag{15}$$

$$\hat{B}_{sy} = \hat{B}_{gm} \frac{\tau_p}{\pi h_{sy}} \tag{16}$$

where τ_s is the slot pitch; b_t and h_{sy} are the tooth width and stator yoke height. The power into the generator winding results from the balance between the absorbed power and iron losses, and it is expressed as

$$P_{wd} = F_{ge} \dot{z} - P_{Fes} \tag{17}$$

where P_{wd} embodies the power taken by the winding of the electrical machine.

In order to achieve higher system efficiency, a back-to-back voltage source inverter is applied for connecting the WEC to the grid (Polinder et al., 2004; Wang et al., 2022d,b). In this inverter, the current I_s is initially regulated to be in phase with the no-load voltage E_p. Thus, the current I_s is calculated as

$$I_s = \frac{P_{wd}}{3E_p} \tag{18}$$

The current I_s is constrained to the maximum current limit of the converter I_{conm}, once it is about to exceed the limit. In these conditions, the terminal voltage U_s can be obtained based on the left phasor diagram shown in Fig. 3.

If the resulting terminal voltage U_s is about to violate the maximum voltage limit U_{conm}, the current I_s is divided into a quadrature (or force-making) component I_{sq} and a direct (or flux making) component I_{sd}. The direct current component I_{sd} could reduce the absolute value of the terminal voltage U_s to comply with the voltage limit. This can be calculated based on the second phasor diagram in Fig. 3. If the resulting current under this condition is larger than the maximum converter current, the operating point is defined by the maximum converter current and voltage. As a consequence, the actual generator force would be less than the required generator force.

After the current I_s is determined the copper losses P_{copper} can be calculated as

$$P_{copper} = 3I_s^2 R_t \tag{19}$$

where R_t is the stator phase resistance. For simplification, the converter losses are assumed to be only related to the generator side in this model, which can be expressed as

$$P_{conv} = \frac{P_{convm}}{31} \left[1 + 20 \frac{I_s}{I_{sm}} + 10 \left(\frac{I_s}{I_{sm}} \right)^2 \right] \tag{20}$$

where P_{conv} is the total converter losses, P_{convm} is the dissipation in the converter at the rated power, and it is assumed to be 3% of the converter's rated power (Polinder et al., 2006); I_{sm} is the magnitude of the maximum generator side current of the converter. In (20), the first term is a small constant part standing for the power dissipated in power supplies, gate drivers, control, and cooling system; the second term accounts for the major part that is proportional to the current, and this part is mainly related to switching losses and conduction losses; the third term is proportional to the current squared, which corresponds to the conduction losses (Polinder et al., 2006). This analytical electrical model has been demonstrated and validated, and more details are provided in Polinder et al. (2004).

It should be acknowledged that, for a stand-alone WEC connected to the DC circuit, the electric load could also make a difference to the power performance of the WEC (Wang et al., 2020). However, in the present work, the linear PM generator is designed to be connected to the electrical grid, as shown in Prado and Polinder (2013). Then it is fair to assume that the electrical grid side is capable of consuming all the power produced by the WEC. Thus, the load variation on the electrical grid is thought to make a negligible difference to the WEC performance.

3.4. Specification of the electric generator

In the present paper, the generator is rated to supply a sufficient force for maximizing power absorption in the most frequent sea state of the sea site Yeu island. The sea state is with the crossing-zero period T_z of 5.5 s and significant wave height H_s of 1 m, as shown in Babarit et al. (2012). The buoy is considered to be semi-submerged during this generator rating process. Fig. 4 shows the relationship between absorbed power, RMS value of the PTO force and PTO damping coefficient at that sea state. It can be observed that a RMS PTO force of 40 kN is required to achieve the maximum absorbed power.

In irregular wave states, the dynamic response of the system is stochastic, and therefore the probability of exceeding the force limit should be maintained within a certain level. For example, PTO force saturation is associated with large currents, and highly frequent PTO force saturation might lead to overheating conditions. Thus, it is essential to define a tolerance on the exceedance during the generator design phase. In this paper, the tolerance on the exceedance of the designed generator force is considered as 10%. If the dynamic process of the WEC is assumed to be Gaussian with zero mean, the amplitude of the variables can be characterized by the Rayleigh distribution (Journée et al., 2015). Hence, the probability of exceeding the PTO force limit can be calculated by

$$P(s) = \exp \left(\frac{-F_m^2}{2\sigma_F^2} \right) \tag{21}$$
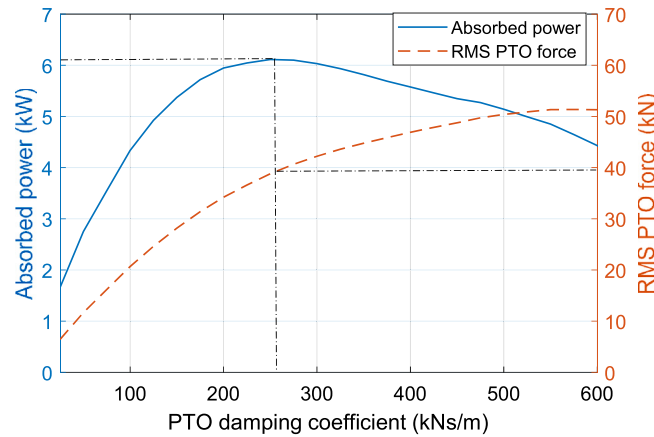
Fig. 4. Absorbed power and RMS PTO force as a function of PTO damping coefficient, with $H_s = 1$ m and $T_z = 5.5$ s.

where σ_F represents the standard deviation of PTO force equaling its RMS value in this case, and F_m is the designed maximum generator force. Given the σ_F of 40 kN, the designed maximum generator force is calculated by (21) as 85 kN.

The size of the linear generator is determined based on the force density of the machine (Tan et al., 2021b, 2022b). The designed maximum generator force is calculated as

$$F_m = 2\rho_{force} L_{sta} l_{sta} \tag{22}$$

where ρ_{force} is the force density of the generator, L_{sta} and l_{sta} are the stator length and stack length, and a factor of 2 is included since the machine is double-sided. The generator adopted in this paper is scaled based on the design of the linear generator of the AWS (Prado and Polinder, 2013). The scale factor of the generator is introduced as

$$\lambda = \frac{S_s}{S_o} \tag{23}$$

where S_s and S_o represent the stator length, the translator length and the stack length of the scaled generator and original generator respectively; subscript 's' and 'o' represent the scaled and original machines. For simplification, the stator, translator and stack length are scaled together in this work while they are in practice independent sizing parameters. As stated in Polinder (2013), the force density is rather constant for differently-sized generators. Therefore, the designed maximum generator force is thought proportional to the active surface area of the machine, and the maximum force of the scaled machine is related to the reference machine by

$$F_{m_s} = \lambda^2 F_{m_o} \tag{24}$$

As in Polinder et al. (2004), the maximum force of the reference generator is 933 kN for two installed machines, and the translator, stator and stack length are reported as 8 m, 5 m and 1 m respectively. As the WEC in this paper only adopts a single machine, then the scale factor λ is calculated as around 0.43. Therefore, the values of the translator, stator and stack length of the scaled machine can be obtained by (23). In addition, the rating of the converter of the scaled generator follows

$$I_{conv_s} = I_{conv_o} \tag{25}$$

$$U_{conv_s} = \lambda^2 U_{conv_o} \tag{26}$$

where I_{conv} and U_{conv} are the rated phase current and voltage of the converter. For the original reference generator, the rated phase current I_{conv_o} and voltage are U_{conv_o} are 400 A and 1500 V (Polinder et al., 2004). Other parameters of the scaled generator remain unchanged with respect to the reference machine, and the specification of the generator used in this paper is shown in Table 1.

Table 1
Specification of the sized generator.

Parameters	Symbol	Quantities
Maximum average power	P_{rared}	187 kW
Maximum force	F_{max}	85 kN
Maximum velocity	u_{max}	2.2 m/s
Displacement limit	S_m	2.8 m
Translator length	L_{tra}	3.5 m
Stator length	L_{sta}	2.2 m
Stack length	l_s	0.45 m
Air gap length	l_g	5 mm
Slot width	b_s	15 m
Magnet pole width	b_p	79 mm
Tooth width	b_t	18.3 mm
Pole pitch	τ_p	100 mm
Slot pitch	τ_s	33.3 mm
Stator yoke height	h_{sy}	50 mm
Slot height	h_s	85 mm
Magnet thickness	l_m	15 mm
Recoil permeability of the magnets	μ_{rm}	1.1
Remanent flux density of the magnets	B_{rm}	1.1 T at 85 °C
Iron loss per unit mass	P_{Fe0}	4.9 W/kg at 50 Hz and 1.5 T
Copper resistivity	ρ_{Cu}	0.0252 μΩm at 120 °C
Copper fill factor	k_{sfil}	0.6
Number of conductors per slot	N_s	6

3.5. Model verification and limitations

The established wave-to-wire model is composed of two main parts, namely the hydrodynamic modeling and the analytical generator modeling. These two main components have been verified or validated respectively in previous work. The hydrodynamic stage of the WEC is modeled by an algebraic nonlinear Froude–Krylov model which has been verified in Giorgi and Ringwood (2017d) and Giorgi and Ringwood (2017a). The analytical electrical generator model used in the current paper is adapted from the model developed for the linear generator of AWS WEC. The original model has been validated by the full-scale test as shown in Polinder et al. (2004).

It has to be noted that the established wave-to-wire model has limited applicability. First, although the algebraic nonlinear Froude–Krylov model is computationally-efficient, it can only be extended to axisymmetric and prismatic geometries of floaters (Giorgi and Ringwood, 2017d). For more complex geometries, the nonlinear Froude–Krylov force has to be calculated by numerical approaches (Penalba et al., 2017b), such as re-meshing panels of instantaneous wetted surface (Lawson et al., 2014). Secondly, as the magnetic saturation was not considered in the analytical electrical modeling, the model is only applicable to operational regions where the stator current is moderate and the magnetic saturation is negligible (Polinder et al., 2004).

3.6. Implementation of numerical modeling

In this work, the wave-to-wire model is implemented in Matlab environment (Matlab 2020) and solved by a numerical integration scheme, that is ODE 45 solver. The fixed time step is used, and it is selected as 0.01 times the considered wave period or peak period in each case. The total simulation length is chosen as 125 times the considered wave period or peak period, and the length of the ramp time is chosen as 25 times the considered wave period or peak period. The calculated responses of the WEC during the period of the ramp time are not taken into account in the analysis. The initial displacement and velocity of the buoy of the WEC are defined as zero. In addition, to efficiently compute the convolution integral of the radiation force, the state-space representation is applied to approximate the term. The state-space parameters and the added mass at the infinite frequency are obtained based on the frequency domain identification method (Pérez and Fossen, 2008). The hydrodynamic coefficients used in this work are calculated by Nemoh which is an open-source numerical tool based on Boundary Element Method (Penalba et al., 2017c).

For the simulation cases applying irregular waves, the JONSWAP spectrum together with a peakedness factor of 3.3 is implemented. Each set of irregular waves is summed up by 500 individual harmonic waves with random phases based on superposition theory (Anon., 2016). The angular frequencies of the harmonic components range from 0.05 π to 4π and are uniformly spaced. To mitigate the random errors resulting from the random phases, each simulation of irregular waves is re-run 10 times and the mean value is subsequently calculated.

4. Results and discussion

This section starts with studying the effect of the draft adjustment on the hydrodynamic feature of the buoy. Then, the wave-to-wire responses of the WEC are presented. Next, the negative effects of the draft adjustment on the buoy motion and partial overlap between the stator and translator of the linear generator are demonstrated. Finally, the performance of the adjustable draft WEC in both regular and irregular waves is identified and compared with the conventional fixed draft WEC. The delivered electrical power, PTO conversion efficiency and the optimal buoy draft in relation to the wave state are covered in the comparison.

4.1. The hydrodynamic features of the adjustable draft WEC

The hydrodynamic analysis of the adjustable draft WEC has been investigated in detail in Tan et al. (2022a). Thus, only two representative proprieties, including the response amplitude operators (RAOs) and absorption bandwidth, are discussed here to highlight the hydrodynamic features of the adjustable draft WEC.

The RAOs of the WEC modeled in the nonlinear model are presented in Fig. 5(a), and the relative error of the linear model to the nonlinear model is shown in Fig. 5(b). As the viscous force and nonlinear Froude–Krylov force are not considered in the linear model, it would result in an overestimation of the motion responses. It is seen that the results of the linear model are clearly deviating from those of the nonlinear model at the wave periods around resonance, and the deviation tends to be more visible with the increase of the buoy draft. It shows the importance of including nonlinear effects, especially when various buoy drafts are involved. Thus, all results presented hereafter are calculated by the nonlinear hydrodynamic model. In addition, it can be observed from Fig. 5 that the natural period of the WEC is highly dependent on the buoy draft, and increasing the buoy draft leads to larger natural periods.

The power absorption bandwidth is a measure reflecting the frequency range within which the WEC could absorb more than half of the maximum power. The relative power absorption of the WEC is calculated for different buoy drafts, as shown in Fig. 6. It can be seen that a disadvantage resulting from increasing the buoy draft is associated with narrower absorption bandwidth. This is mainly because the buoy mass is increased by enlarging the buoy draft (Tan et al., 2022a).

### 4.2. Wave-to-wire responses of the WEC

The systematic responses of the WEC calculated by the established wave-to-wire model are presented in Figs. 7 and 8, in which the buoy draft is selected to be 4.0 m as an example. A mild wave state and a powerful wave state are considered respectively. The profiles of the RMS no-load voltage in Figs. 7(b) and 8(b) are not sinusoidal because of the partial overlap between the stator and translator of the generator. As a consequence, the resulting phase current and terminal voltage in Figs. 7(c) and 8(c) are not varying sinusoidally either. The effect is more obvious in the powerful wave state, where the amplitude of the displacement is larger. In addition, in Fig. 8(c), it is seen the profiles of the voltage and current are not symmetrical with respect to the dashed center line of a half oscillation period. Because the geometry center of the translator in still water is not located parallel to the vertical center line of the stator. This results in the difference in the duration of the partial overlap between the buoy's moving upwards and downwards. This effect will be demonstrated in detail in Section 4.3. Furthermore, it can be found from Figs. 7(d) and 8(d) that copper losses account for a major proportion of electrical losses during energy conversion in this case.

4.3. Negative effects of the draft adjustment

In the current concept, the buoy and translator are connected in a rigid way. Then, two effects need to be considered after the adjustable draft system is adopted. Firstly, the draft adjustment makes the stroke of the buoy non-symmetrical, and thus the end-stop force takes effect on one side earlier than on the other side. Secondly, the draft adjustment makes the duration of the partial overlap between the stator and translator non-symmetrical, which affects the profile of the induced voltage and current. Fig. 9 illustrates how the relative position of the buoy and translator to the stator changes with the buoy draft. It can be seen that the displacement limits of the adjustable draft WEC, except for the buoy draft of 4.25 m, are not symmetrical with respect to the horizontal center line of the stroke. Thus, when the buoy draft is adjusted to be smaller than 4.25 m, the distance between the top of the moving parts and the upper end of the stroke is less than that between the bottom of the moving parts to the lower end of the stroke. The effect is vice-verse for cases with buoy drafts larger than 4.25 m. In addition to stroke, it is seen that if the buoy draft is smaller than 4.25 m, the overlap between the translator and stator is reduced when the buoy moves in an upwards direction. The following two subsections are intended to demonstrate these two effects on the responses as well as the power performance of the WEC.

4.3.1. The effect on the stroke

Fig. 10 shows the ratio of the maximum displacement of the semi-submerged fixed draft WEC to that of the adjustable draft WEC with the buoy draft adjusted to 3.5 m. Fig. 11 shows the ratio between the absorbed power of these two WECs. In the calculation, different motion limits are considered, ranging from $0.6R$ to $1.0R$. The fixed draft WEC is a good reference for comparison, since it is not subjected to the effect of non-symmetrical stroke. It can be seen that, for mild wave states or large motion limits, the influence is highly limited. However, it is noticeable for cases with short motion limits and large wave heights. The displacement ratio (in Fig. 10) and power ratio (in Fig. 11) even reach 1.14 and 1.07 respectively when the motion limit is $0.6R$ and wave height is 4 m. The longer strokes could mitigate this effect, but the cost is also correspondingly higher. Thus, the motion limit is selected as $0.8R$ in the current design of the adjustable draft WEC as a compromise. However, it is acknowledged that the non-symmetry stroke effect on the response of the WEC could be more remarkable if the motion is amplified by real-time control strategies.
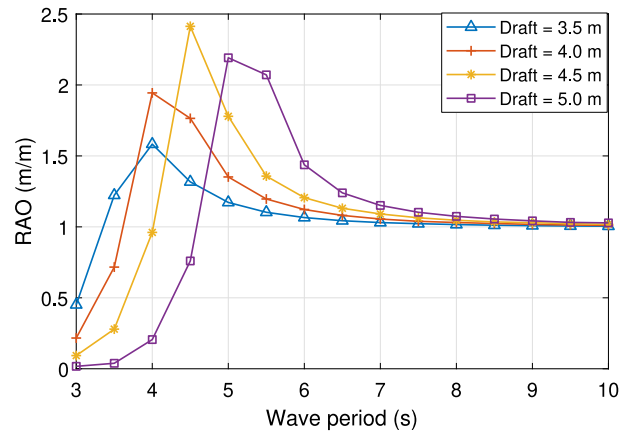
(a) RAOs predicted by the established nonlinear model, and $H = 1$ m.
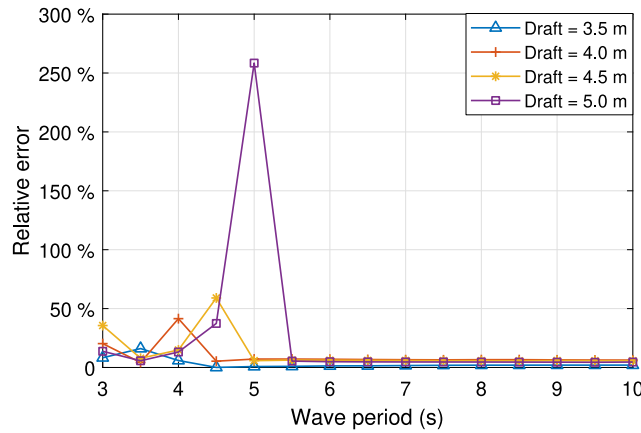
(b) The relative error of the linear model to the nonlinear model.

Fig. 5. The RAOs prediction of the established nonlinear model and the relative error of the linear model to the nonlinear model.
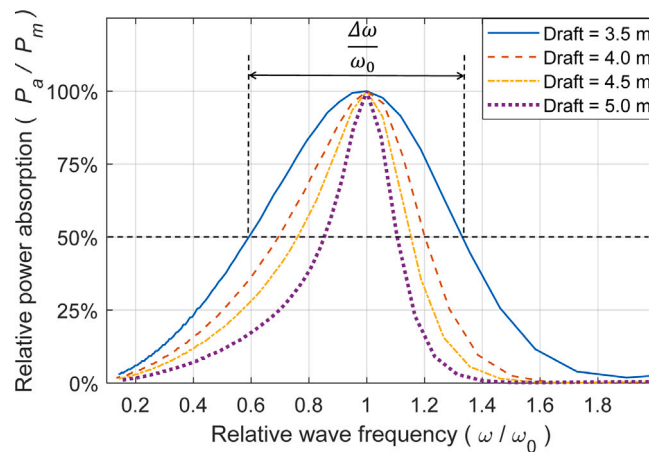

Fig. 6. The relative power absorption of the WEC with different buoy drafts calculated by the nonlinear model, and $H = 1$ m. The PTO damping is tuned to maximize the absorbed power at the wave period of $T = 5.5$ s.

4.3.2. The effect on the partial overlap

The buoy draft adjustment makes a difference to the duration of the overlap between the stator and translator, as depicted in Fig. 9. In Fig. 12, the RMS no-load voltage and phase current profiles of the semi-submerged fixed draft WEC and adjustable draft WEC are compared, in which the buoy draft of the adjustable draft WEC is adjusted to 3.5 m in this case. It is visible in Fig. 12(a) that the adjustable draft WEC has a lower RMS no-load voltage profile than the fixed draft WEC over a proportion of each oscillation. This is because the upper part of the translator T_u is larger than T_l in the case with the draft of 3.5 m as shown in Fig. 9. The complete overlap of the adjustable draft WEC is, therefore, shorter when the buoy is moving in an upwards direction, and then the resulting no-load voltage is lower than the fixed draft WEC. As a consequence, the phase current needs to be correspondingly increased for supplying the required generator force, as is shown in Fig. 12(b).
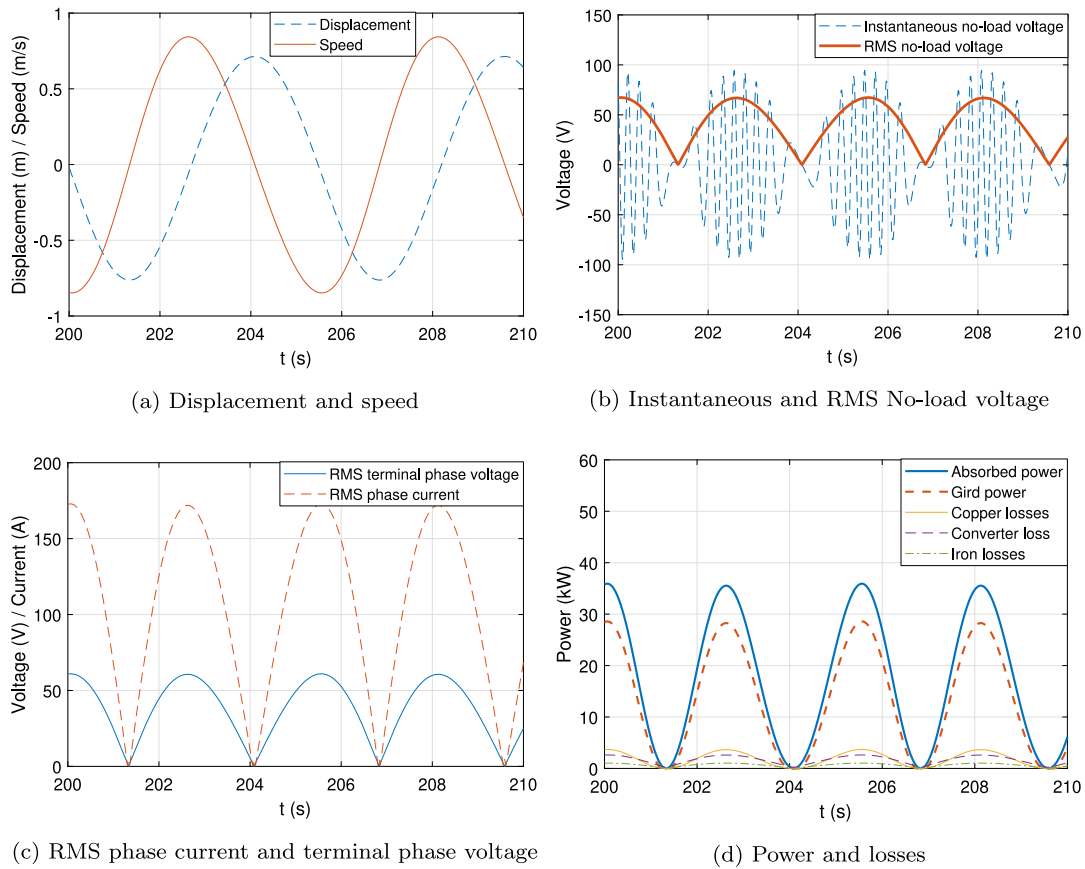
(a) Displacement and speed

(b) Instantaneous and RMS No-load voltage

(c) RMS phase current and terminal phase voltage

(d) Power and losses

Fig. 7. Wave-to-wire response of the WEC in a mild wave state (H = 1.5 m, T = 5.5 s), and B_{pto} = 50 kNs/m.

The effect of the non-symmetrical partial overlap on the power generation in different wave periods and heights is depicted in Fig. 13. The electrical power of the fixed draft WEC is normalized to that of the adjustable draft WEC. It can be seen that the effect generally tends to be stronger with the increase of the wave height. In addition, the normalized power ratio slightly decreases from the wave height of 3.5 m to 4 m for the wave period of 5 s. It can be explained by the fact that the partial overlap comes to play in both upwards and downwards buoy motion in large wave heights, and the adjustable draft WEC has a longer duration of the complete overlap in the downwards motion. Fig. 14 depicts that enlarging the translator length could effectively mitigate the effect of the non-symmetrical overlap. For instance, increasing the translator length from 3.2 m to 4 m could reduce the normalized power ratio from 1.05 to 1.01 at the wave height of 1.5 m. However, longer translators imply more materials and thus a higher cost on the generator, and a compromise needs to be made for this issue. In the current design of the adjustable draft WEC, the translator length is determined as 3.5 m.

4.4. Performance identification

The power performance of the adjustable draft WEC is demonstrated in this part. It is assumed that the buoy draft can always be suitably and effectively adjusted to each wave state for maximizing the delivered power. The power performance of the WEC with the fixed buoy draft of 3.5 m, namely the semi-submerged WEC, is also presented for comparison.

4.4.1. PTO damping optimization

The PTO damping is important to power extraction. However, the optimal PTO damping for the absorbed mechanical power is not necessarily associated with the maximum electrical power since the influence

of the PTO damping on the generator efficiency also plays a role (Coe et al., 2021). In Fig. 15, the relationship between the PTO damping, absorbed power, electrical power and generator efficiency is depicted. The maximum generator efficiency is 70% and it occurs at the PTO damping of around 25 kNm/s. However, the maximum absorbed power is obtained at the PTO damping of 150 kNm/s which is associated with the generator efficiency of approximately 45%. So, there is an obvious mismatch, and the maximization of the absorbed power does not necessarily result in the maximum delivered electrical power. As a collective consequence of the generator efficiency and absorbed power, the optimal PTO damping corresponding to the maximum electrical power is 100 kNm/s. In this case, the deviation of the PTO damping optimal to the absorbed power from that optimal to the electrical power reaches 50%.

Fig. 16 shows the influence of the PTO damping on the proportion of losses. It could explain the tendency of the generator efficiency with the PTO damping shown in Fig. 15. At very small PTO damping coefficients, the iron losses make up a major part of the total losses. This is because the movement speed of the translator is high, which results in high generator frequencies. The iron losses are directly related to the generator frequency. With the increase of the PTO damping coefficient, the required PTO force increases, but the movement speed decreases. Thus, the no-load voltage decreases and the current has to be improved to a higher level to supply the required generator force. In this way, copper losses tend to be more relevant. This explains why the generator efficiency tends to first increase and then decrease with the PTO damping coefficient.

It can be noticed that the generator efficiency is strongly related to the PTO parameters. Optimizing the PTO damping for the absorbed power is clearly insufficient for the maximization of the final delivered power output, namely the delivered electrical power. Hereafter, the power performance of the adjustable draft WEC is identified based on the optimized PTO damping for the delivered electrical power.
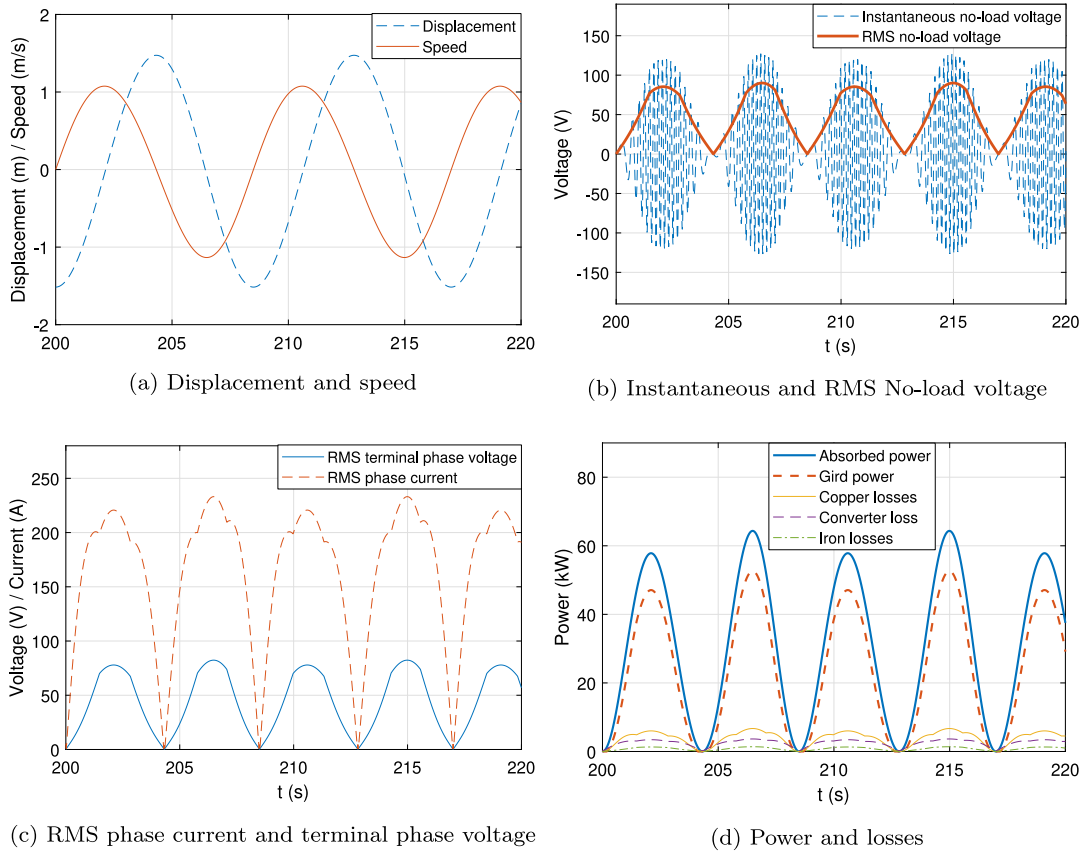
(a) Displacement and speed

(b) Instantaneous and RMS No-load voltage

(c) RMS phase current and terminal phase voltage

(d) Power and losses

Fig. 8. Wave-to-wire response of the WEC in a powerful wave state ($H = 3.0$ m, $T = 8.5$ s), and $B_{pto} = 50$ kNs/m.
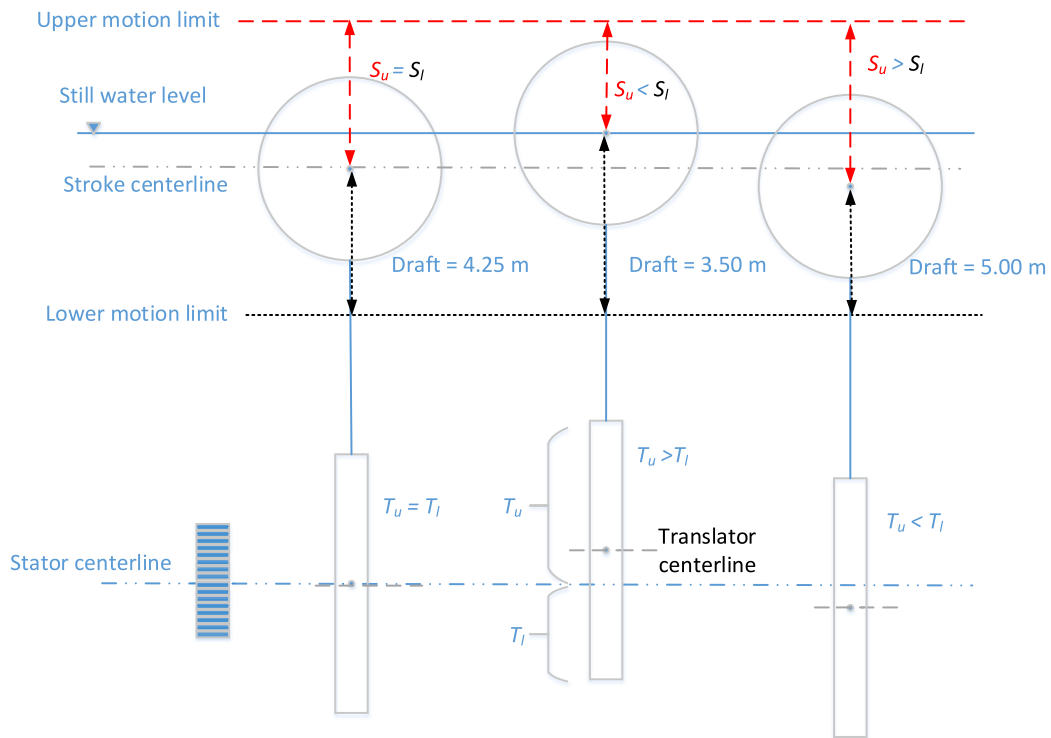

Fig. 9. The schematic of the relative positions of the buoy, translator and stator in different buoy drafts. S_u and S_l represent the upper and lower part of the stroke relative to the buoy centroid. T_u and T_l represent the upper and lower part of the translator relative to the center line of the stator.
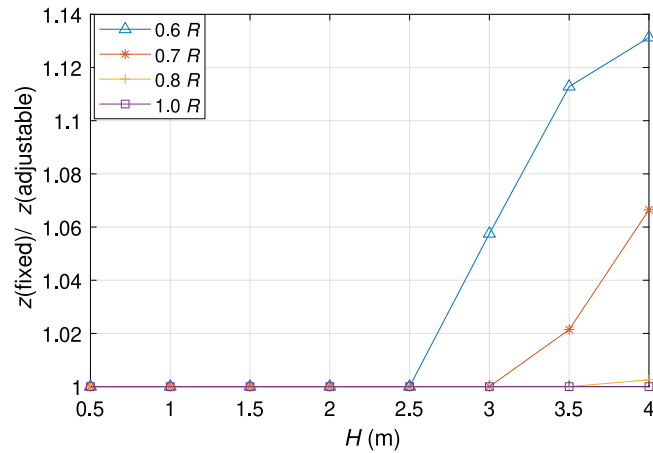
Fig. 10. The maximum displacement of the fixed draft WEC with the draft of 3.5 m normalized to that of the adjustable draft WEC with the draft of 3.5 m at the undamped condition, and $T = 5.0$ s. The considered motion limits range from $0.6R$ to $1.0R$.
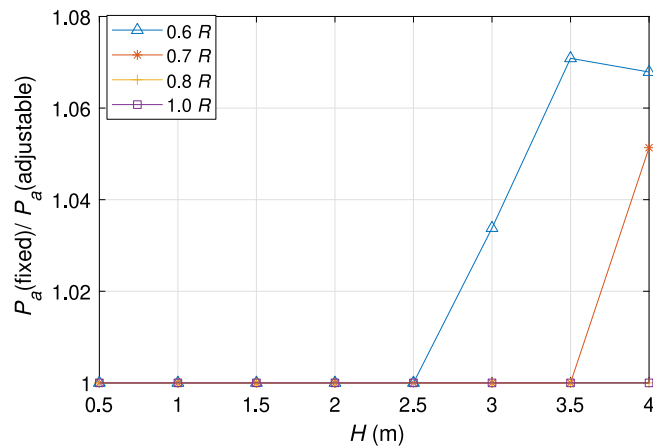
Fig. 11. The average absorbed power of the fixed draft WEC with the draft of 3.5 m normalized to that of the adjustable draft WEC with the draft of 3.5 m, and $B_{pto} = 30$ kNs/m and $T = 7.0$ s. The considered motion limits range from $0.6R$ to $1.0R$.

4.4.2. In regular waves

The delivered electrical power of the adjustable draft WEC is calculated for regular wave conditions, as shown in Fig. 18. For comparison, the power performance of the semi-submerged fixed draft WEC is also presented in the figure. It can be seen that the adjustable draft WEC is associated with a higher power output over a range of wave periods. This mainly results from the increased buoy velocity, which is depicted in Fig. 17. The gain of the power resulting from the adjustable draft system is mainly observed from the wave period of 4 s to 6 s. For instance, the highest power for the adjustable draft WEC is around 47 kW at the period of 4.5 s while it is only around 38 kW for the fixed draft WEC. The improvement is as high as 24%. When the wave period is below 4 s or above 6 s, the adjustable draft WEC and fixed draft WEC tend to deliver a similar amount of electrical power.

The electrical losses and the overall generator efficiencies are calculated for the adjustable draft WEC and the fixed draft WEC respectively, as shown in Fig. 19. It is reflected that the copper losses and converter losses make up the major losses in the power conversion stage of this generator. The maximum values of the copper losses, converter losses and iron losses are approximately 5 kW, 3 kW and 1 kW respectively. When the wave periods are below 4 s, the adjustable draft WEC presents larger copper and converter losses and the fixed draft WEC has a slightly higher generator efficiency than the adjustable draft WEC. This mainly results from the negative effects of the draft adjustment on the symmetry of the stroke and the partial overlap between the stator and translator, which causes a larger current in the generator and further

larger copper and converter losses. At the wave periods from 4 s to 6.5 s, the increased generator efficiencies of the adjustable draft WEC result from the larger buoy velocity. During these wave periods, the iron losses of the adjustable draft WEC overtake those of the fixed draft WEC due to the higher buoy velocity, and the adjustable draft WEC is associated with relatively higher copper and converter losses than the fixed draft WEC. But, given the significantly larger power absorption, the adjustable draft WEC shows a higher generator efficiency than the fixed draft WEC. For instance, at the wave period of 4.5 s, the generator efficiency of the adjustable draft WEC is 83% while it is 80% for the fixed draft WEC. When the wave period is beyond 7 s, there is not any noticeable difference observed between the generator efficiencies of the adjustable draft WEC and fixed draft WEC.

To comprehensively reveal the potential of the adjustable draft system, the performance of the adjustable draft WEC is calculated in different wave states. The electrical power of the adjustable draft WEC is normalized to that of the fixed draft WEC, as shown in Fig. 20. It can be seen that the normalized value is obviously higher than one over various wave heights. This implies that the adjustable draft system could lead to higher power production in a broad range of operational regions. Secondly, it is visible that the normalized value first tends to decrease and then tends to be relatively constant with the increase in wave height. This can be attributed to two aspects. First, the adjustable draft WEC is associated with higher velocity, and the viscous drag force is proportional to the velocity squared. As the increase of the wave height results in larger velocity as well as the drag force, the power
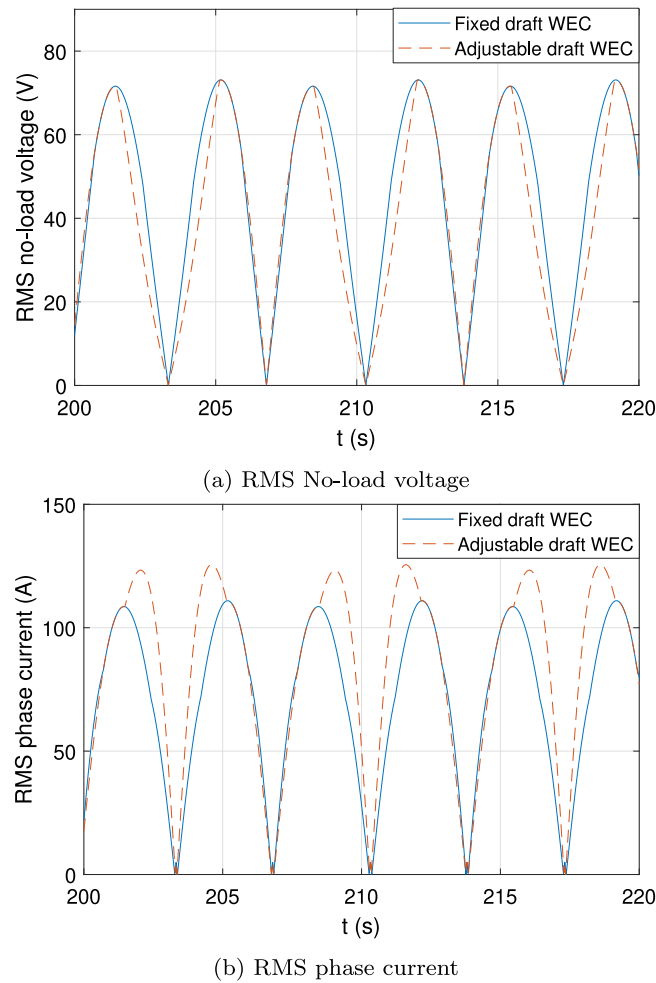
(a) RMS No-load voltage

(b) RMS phase current

Fig. 12. The effect of the non-uniform partial overlap on the profile of generator responses, and $H = 2$ m, $T = 7$ s and $B_{pto} = 30$ kNs/m.
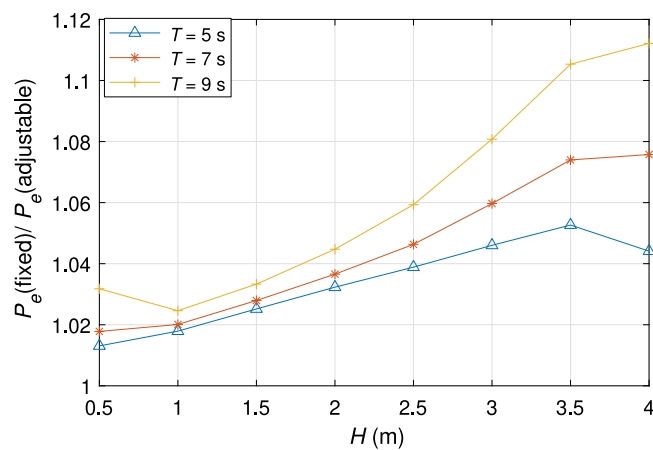

Fig. 13. The average electrical power of the fixed draft WEC with the draft of 3.5 m normalized to that of the adjustable draft WEC with the draft of 3.5 m, and $B_{pto} = 30$ kNs/m.

absorption of the adjustable draft WEC is relatively more penalized by the viscous drag force. Secondly, the defined force limit is not taking effect in low wave heights. Then, the velocity of the adjustable draft WEC is not constrained, and it can be much higher than that of the fixed draft WEC. Because the adjustable draft system is able to tune the natural period to the incoming waves. Thus, the improvement of the power production resulting from the adjustable draft system is more pronounced in low wave height.

4.4.3. In irregular waves

Fig. 22 shows the standard deviation of the buoy velocity in irregular wave states, and the adjustable draft WEC contributes to a higher velocity within the peak periods between 4.5 s and 6.5 s. For instance, at the peak period of 5 s, the standard deviation of the buoy velocity is 0.69 m/s and 0.74 m/s for the fixed draft WEC and the adjustable draft WEC respectively. The electrical power delivered by the adjustable draft WEC and the fixed draft WEC in irregular wave states is presented in Fig. 21. It can be seen that the power improvement resulting from
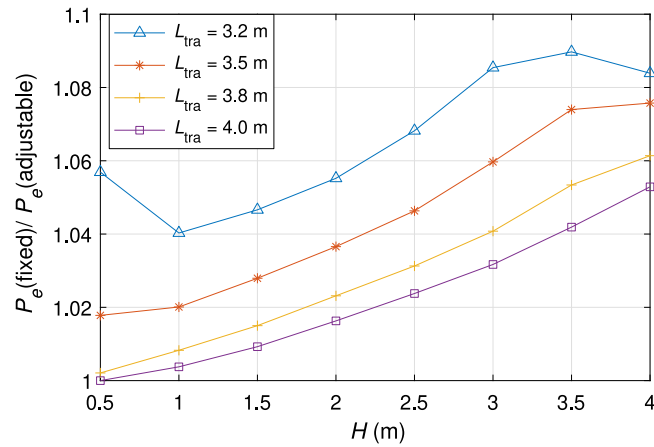
Fig. 14. The average electrical power of the fixed draft WEC with the draft of 3.5 m normalized to that of the adjustable draft WEC with the draft of 3.5 m in wave states of $T = 7.0$ s, and $B_{pto} = 30$ kNs/m. Different values of the translator length L_{tra} are considered.
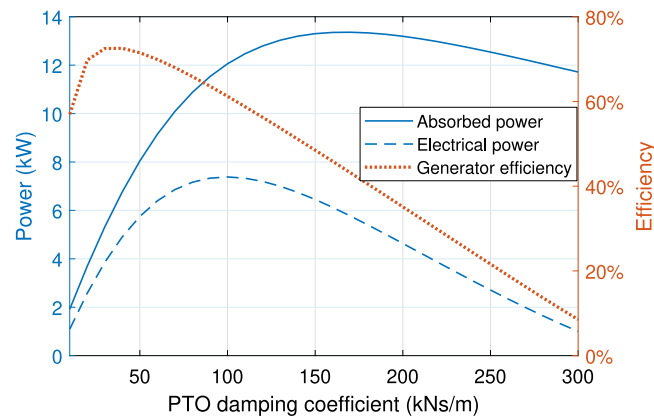

Fig. 15. The absorbed power and generator efficiency of the WEC with the buoy draft of 3.5 m as a function of the PTO damping coefficient, and $H = 1$ m and $T = 5.5$ s.
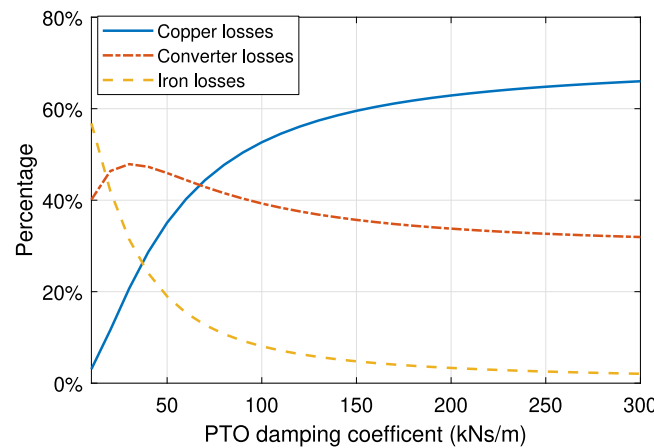

Fig. 16. The percentage of different types of losses to the total losses of the WEC with the buoy draft of 3.5 m as a function of the PTO damping coefficient, and $H = 1$ m and $T = 5.5$ s.

the adjustable draft system in irregular waves is less noticeable than that in regular waves. The highest values of the electrical power for the fixed draft WEC and adjustable draft WEC are approximately 22 kW and 24.5 kW, and the improvement is around 10%. When the peak period is above 6.0 s, the difference between the electrical power output of the adjustable draft WEC and the fixed draft WEC is negligible. This is because increasing the buoy draft reduces the absorption bandwidth of the buoy, and the narrower bandwidth reflects the incapability in responding to broad wave frequencies other than the natural frequency.

Therefore, the power absorption of the buoy with larger buoy drafts in irregular waves is weakened with regard to that in regular wave states.

Fig. 23 shows the generator efficiencies of the adjustable draft WEC and fixed draft WEC in irregular wave states. the adjustable draft WEC presents comparable generator efficiencies with the fixed draft WEC when the peak period is higher than 4.5 s. At the peak period below 4.5 s, the fixed draft WEC is clearly associated with a higher generator efficiency. For instance, at the peak period of 3.5 s, the generator
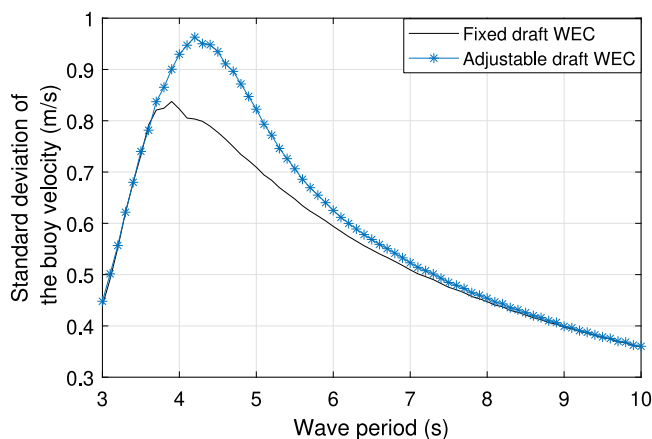
Fig. 17. Standard deviation of the buoy velocity of the adjustable draft WEC and of the fixed draft WEC, with $H = 2$ m and $\sigma_F = 40$ kN.
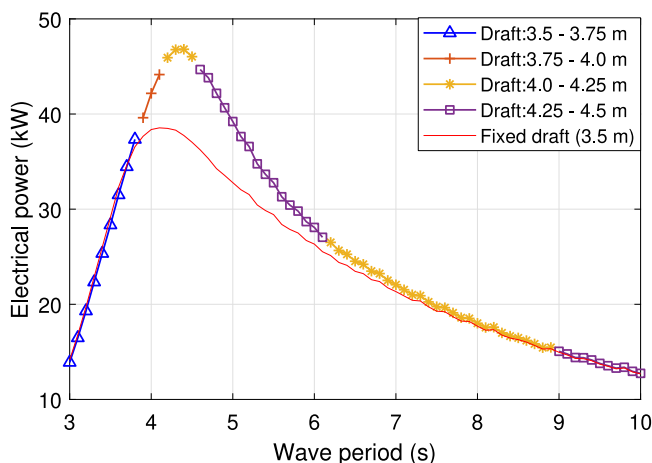

Fig. 18. Comparison between the delivered electrical power of the adjustable draft WEC and of the fixed draft WEC, with $H = 2$ m and $\sigma_F = 40$ kN.

efficiency is 74% for the fixed draft WEC, while it is only 70% for the adjustable draft WEC. This can be attributed to the negative effects of the draft adjustment on the symmetry of the stroke and the overlap between the translator and stator.

4.5. Performance of the improved concept of the adjustable draft WEC

The non-symmetry of the stroke and partial overlap between the translator and stator resulting from the draft adjustment has a negative effect on the power extraction and generation. To mitigate the effects, one possibility is to install a mooring winch inside the buoy to adjust the available length of the connecting rope, and this is a suitable flexible connection between the buoy and the translator. The winch fraps or releases the connecting rope to suit the set-up of the buoy draft, by which the center line of the translator and stator can always be aligned with each other in the still water level. The schematic of the improved concept is shown in Fig. 24. Another possibility has been mentioned in Tan et al. (2022a) for a rigid connection between the buoy and the translator, in which a hydraulic clamp is installed inside the buoy to adapt the effective length of the connecting rod correspondingly to the draft adjustment. Both of these two types of designs could eliminate the non-symmetrical issue resulting from the draft adjustment.

The generator efficiency of the improved adjustable draft WEC is shown in Fig. 25. Compared with the original design, the delivered electrical power is increased during the low peak wave periods from 3.5 s to 4.5 s. When the peak period is higher than 4.5 s, the generator efficiencies between the improved designs and the original

designs are comparable. Nevertheless, either the mooring winch or the hydraulic clamp would consume extra energy, which also reduces the net delivered energy of the WEC. In addition, it is acknowledged that the addition of equipment could also increase capital expenditure and maintenance demand. As for its economic viability in practice, a comprehensive techno–economic analysis, as in De Andres et al. (2016), is demanded as support for making further decisions.

5. Summary and conclusion

In this paper, a wave-to-wire model is established to investigate the system performance of a newly proposed WEC concept, namely the adjustable draft WEC. The established model integrates a nonlinear hydrodynamic model with an analytical model for a linear PM generator. The nonlinear Froude–Krylov force and viscous force are covered. The generator is rated for the most frequent wave state in a sea site of interest. The negative effects of the draft adjustment on the stroke and partial overlap between the stator and translator of the generator are analyzed. The performance of the proposed WEC is studied for both regular and irregular wave conditions. The following conclusions are drawn.

Firstly, the draft adjustment leads to the non-symmetry of the stroke and partial overlap of the generator, which could reduce the power absorption and conversion efficiency of the system. Increasing the stroke and translator length could effectively mitigate these effects. However, these negative effects could be mitigated by increasing the stroke and translator length, but the cost will also be higher. With
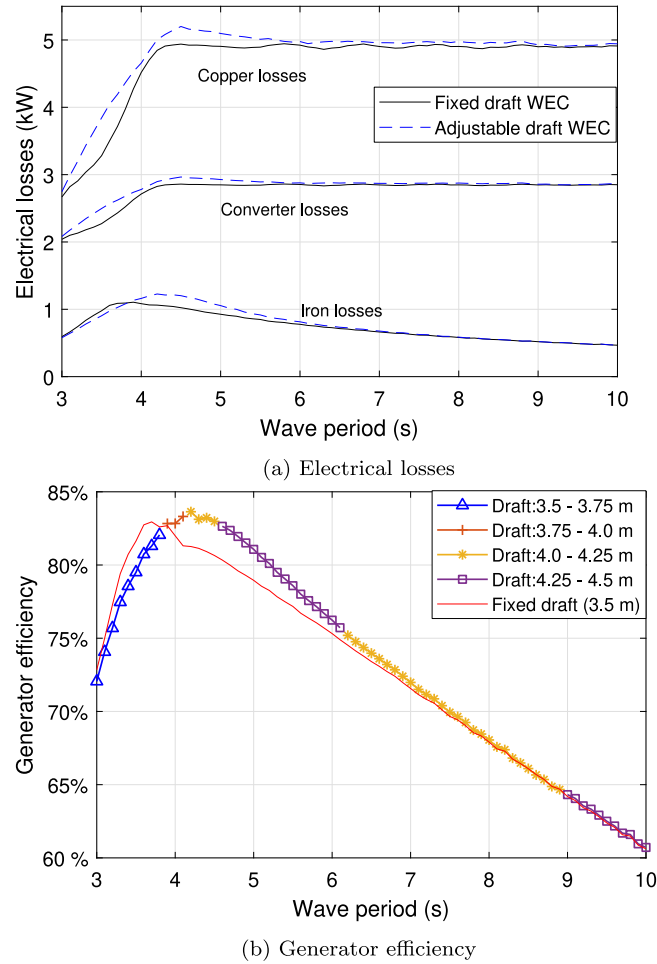
(a) Electrical losses

(b) Generator efficiency

Fig. 19. Comparison between the generator performance of the adjustable draft WEC and of the fixed draft WEC, with $H = 2$ m and $\sigma_F = 40$ kN.
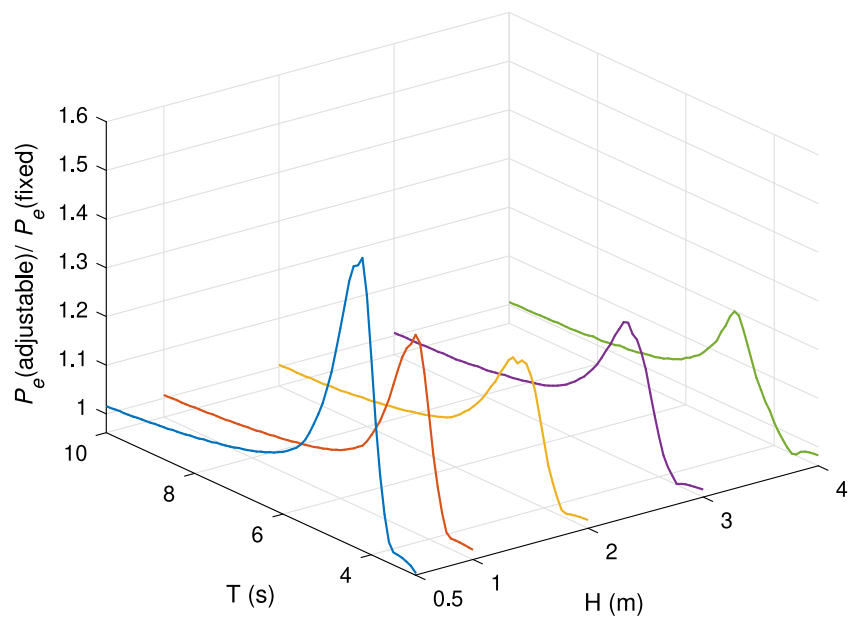

Fig. 20. The electrical power of the adjustable draft WEC normalized to that of the fixed draft WEC in various wave states.
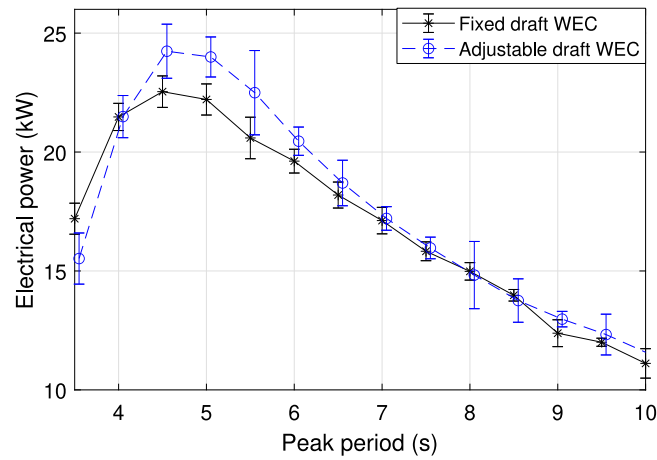
Fig. 21. Comparison between the delivered electrical power of the adjustable draft WEC and of the fixed draft WEC, with $H_s = 2.5$ m and $\sigma_F = 40$ kN. The shaded area represents the standard deviation.
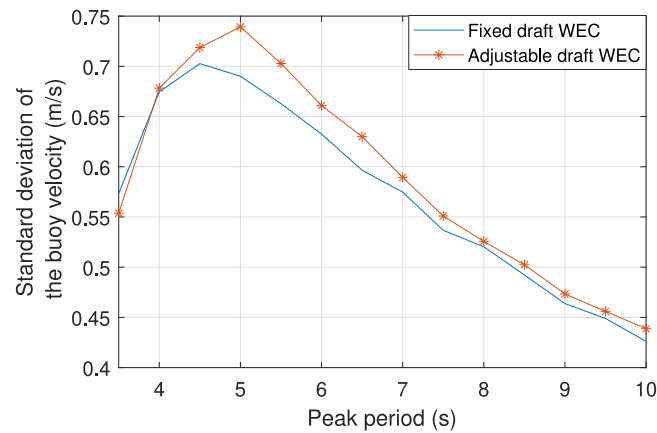

Fig. 22. Standard deviation of the buoy velocity of the adjustable draft WEC and of the fixed draft WEC, with $H_s = 2.5$ m and $\sigma_F = 40$ kN.
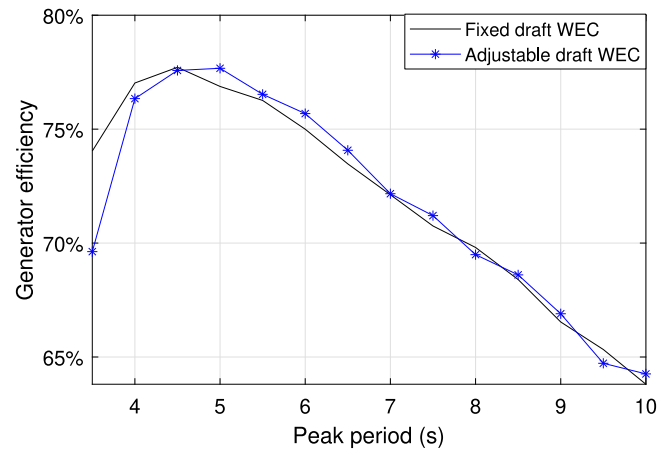

Fig. 23. Comparison between the generator efficiency of the adjustable draft WEC and of the fixed draft WEC, with $H_s = 2.5$ m and $\sigma_F = 40$ kN.

regard to the specified device in this paper, the negative effects on the power absorption and generator efficiency are not significant.

Secondly, the wave-to-wire model reveals the fact that the maximization of the absorbed power and the electrical power results in significantly different selections of the PTO damping coefficients. In this particular case, the difference between the resulting PTO damping coefficients is 50%. The PTO damping coefficient optimal for maximizing the absorbed power is larger than that for maximizing the

electrical power, due to higher copper losses. It indicates the importance to incorporate the variation of PTO efficiency during tuning PTO parameters.

Thirdly, compared with the conventional fixed draft WEC, the adjustable draft WEC is beneficial for power production over a range of wave periods in spite of the negative effects of the draft adjustment. The maximum improvement of delivered electrical power is around 24% in regular wave states. Besides, the generator efficiency of the
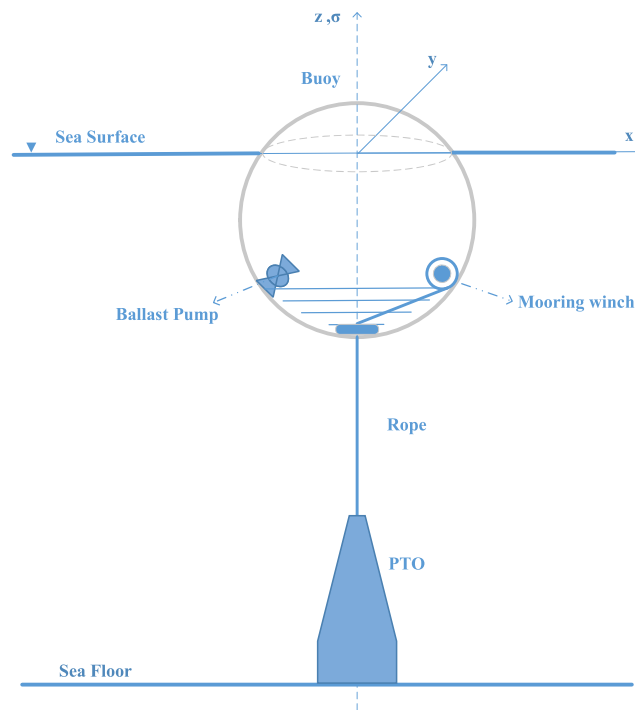
(a) With a mooring winch
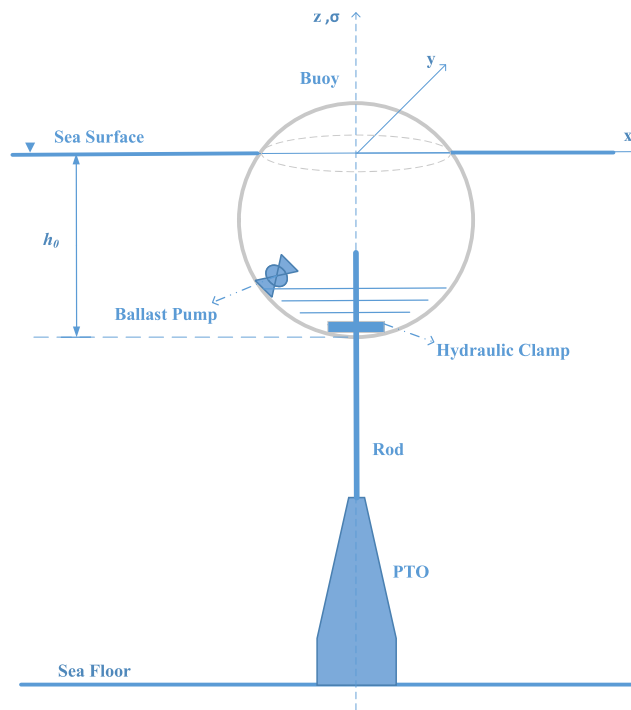
(b) With a hydraulic clamp

Fig. 24. Schematic of the improved adjustable draft point absorber.

adjustable draft WEC is higher than the fixed draft WEC for some particular wave periods since the adjustable draft WEC could contribute to the increased buoy velocity. At very low wave periods, the generator efficiency of the adjustable draft WEC is lower because of the negative effects resulting from the draft adjustment. In irregular wave states, the power improvement by applying the adjustable draft system is reduced because the semi-submerged fixed draft WEC has wider absorption bandwidth than the buoy with larger drafts. Nevertheless, a 10% gain in electrical power can be achieved by using the adjustable draft system in particular wave states.
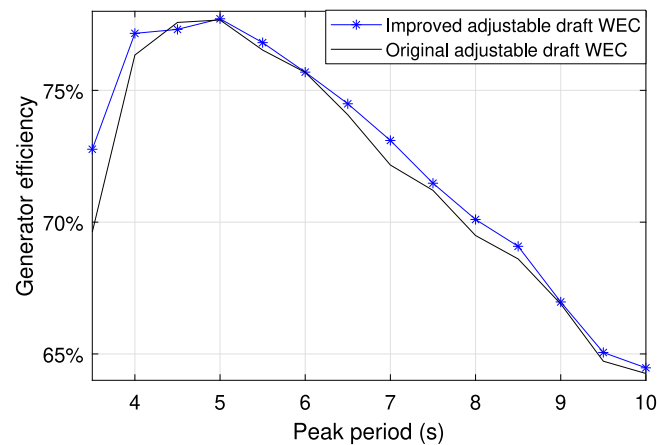
Fig. 25. Comparison between the generator efficiency of the improved adjustable draft WEC and the original adjustable draft WEC, with $H_s = 2.5$ m and $\sigma_F = 40$ kN.

CRediT authorship contribution statement

Jian Tan: Conception and design of study, Acquisition of data, Analysis and/or interpretation of data, Writing – original draft, Writing – review & editing. **Henk Polinder:** Conception and design of study, Writing – review & editing. **Antonio Jarquin Laguna:** Conception and design of study, Writing – review & editing. **Sape Miedema:** Conception and design of study, Writing – review & editing.

Declaration of competing interest

The authors declare that they have no known competing financial interests or personal relationships that could have appeared to influence the work reported in this paper.

Data availability

Data will be made available on request.

References

Aderinto, T., Li, H., 2018. Ocean wave energy converters: Status and challenges. Energies 11, 1–26.

Anon., 2016. Numerical modelling of wave energy converters.

Babarit, A., Hals, J., Muliawan, M.J., Kurniawan, A., Moan, T., Krokstad, J., 2012. Numerical benchmarking study of a selection of wave energy converters. Renew. Energy 41, 44–63.

Bailey, H., Robertson, B.R.D., Buckham, B.J., 2016. Wave-to-wire simulation of a floating oscillating water column wave energy converter. Ocean Eng. 125, 248–260.

Benreguig, P., Kelly, J., Pakrashi, V., Murphy, J., 2019. Wave-to-wire model development and validation for two OWC type wave energy converters. Energies 12, 3977.

Ciappi, L., Cheli, L., Simonetti, I., Bianchini, A., Manfrida, G., Cappietti, L., 2020. Wave-to-wire model of an oscillating-water-column wave energy converter and its application to mediterranean energy hot-spots. Energies 13, 5582.

Ciappi, L., Cheli, L., Simonetti, I., Bianchini, A., Talluri, L., Cappietti, L., Manfrida, G., 2022a. Wave-to-wire models of wells and impulse turbines for oscillating water column wave energy converters operating in the Mediterranean sea. Energy 238, 121585.

Ciappi, L., Simonetti, I., Bianchini, A., Cappietti, L., Manfrida, G., 2022b. Application of integrated wave-to-wire modelling for the preliminary design of oscillating water column systems for installations in moderate wave climates. Renew. Energy 194, 232–248.

Clemente, D., Rosa-Santos, P., Taveira-Pinto, F., 2021. On the potential synergies and applications of wave energy converters: A review. Renew. Sustain. Energy Rev. 135, 110162.

Coe, R.G., Bacelli, G., Forbush, D., 2021. A practical approach to wave energy modeling and control. Renew. Sustain. Energy Rev. 142, 110791.

Colby, M.K., Nasroullahi, E.M., Tumer, K., 2011. Optimizing ballast design of wave energy converters using evolutionary algorithms. In: Proceedings of the 13th Annual Conference on Genetic and Evolutionary Computation. pp. 1739–1746.

Cummins, W.E., Iiuhl, W., Uinm, A., 1962. The impulse response function and ship motions.

De Andres, A., Maillet, J., Todalshaug, J.H., Möller, P., Bould, D., Jeffrey, H., 2016. Techno–economic related metrics for a wave energy converters feasibility assessment. Sustainability 8.

De Andres, A., Medina-Lopez, E., Crooks, D., Roberts, O., Jeffrey, H., 2017. On the reversed LCOE calculation: Design constraints for wave energy commercialization. Int. J. Mar. Energy 18, 88–108.

Falcão, A.F.O., 2010. Wave energy utilization: A review of the technologies. Renew. Sustain. Energy Rev. 14, 899–918.

Falnes, J., 2003. Ocean Waves and Oscillating Systems.

Flocard, F., Finnigan, T.D., 2012. Increasing power capture of a wave energy device by inertia adjustment. Appl. Ocean Res. 34, 126–134.

Forehand, D.I., Kiprakis, A.E., Nambiar, A.J., Wallace, A.R., 2015. A fully coupled wave-to-wire model of an array of wave energy converters. IEEE Trans. Sustain. Energy 7, 118–128.

Giorgi, G., Ringwood, J.V., 2017a. Computationally efficient nonlinear Froude–Krylov force calculations for heaving axisymmetric wave energy point absorbers. J. Ocean Eng. Mar. Energy 3, 21–33.

Giorgi, G., Ringwood, J.V., 2017b. Consistency of viscous drag identification tests for wave energy applications. In: 12th European Wave and Tidal Energy Conference. pp. 1–8.

Giorgi, G., Ringwood, J.V., 2017c. Importance of nonlinear wave representation for nonlinear Froude–Krylov force calculations for wave energy devices. In: Proceedings of the 12th European Wave and Tidal Energy Conference.

Giorgi, G., Ringwood, J.V., 2017d. Nonlinear Froude–Krylov and viscous drag representations for wave energy converters in the computation/fidelity continuum. Ocean Eng. 141, 164–175.

Gurnari, L., Filianoti, P.G., Torresi, M., Camporeale, S.M., 2020. The wave-to-wire energy conversion process for a fixed U-OWC device. Energies 13, 283.

Josset, C., Babarit, A., Clément, A.H., 2007. A wave-to-wire model of the SEAREV wave energy converter. Proc. Inst. Mech. Eng. M 221, 81–93.

Journée, J.M.J., Massie, W.W., Huijsmans, R.H.M., 2015. Offshore Hydrodynamics.

Kelly, J.F., Wright, W.M., Sheng, W., O'Sullivan, K., 2015. Implementation and verification of a wave-to-wire model of an oscillating water column with impulse turbine. IEEE Trans. Sustain. Energy 7, 546–553.

Lawson, M., Yu, Y.-H., Nelessen, A., Ruehl, K., Michelen, C., 2014. Implementing nonlinear buoyancy and excitation forces in the WEC-Sim wave energy converter modeling tool. In: International Conference on Offshore Mechanics and Arctic Engineering, vol. 45547. American Society of Mechanical Engineers, V09BT09A043.

Lehmann, M., Karimpour, F., Goudey, C.A., Jacobson, P.T., Alam, M.R., 2017. Ocean wave energy in the United States: Current status and future perspectives. Renew. Sustain. Energy Rev. 74, 1300–1313.

Liu, Z., Wang, X., Al Shami, E., Baker, N.J., Ji, X., 2021. A study of a speed amplified linear generator for low-frequency wave energy conversion. Mech. Syst. Signal Process. 149, 107226.

Liu, Z., Xu, C., Kim, K., 2022. A CFD-based wave-to-wire model for the oscillating water column wave energy convertor. Ocean Eng. 248, 110842.

Penalba, M., Cortajarena, J.-A., Ringwood, J.V., 2017a. Validating a wave-to-wire model for a wave energy converter—Part II: The electrical system. Energies 10, 1002.

Penalba, M., Giorgi, G., Ringwood, J.V., 2017b. Mathematical modelling of wave energy converters: A review of nonlinear approaches. Renew. Sustain. Energy Rev. 78, 1188–1207.

Penalba, M., Kelly, T., Ringwood, J., 2017c. Using NEMOH for modelling wave energy converters : A comparative study with WAMIT. In: 12th European Wave and Tidal Energy Conference. p. 10.

Penalba, M., Ringwood, J.V., 2019. A high-fidelity wave-to-wire model for wave energy converters. Renew. Energy 134, 367–378.

Penalba, M., Sell, N.P., Hillis, A.J., Ringwood, J.V., 2017d. Validating a wave-to-wire model for a wave energy converter—Part I: The hydraulic transmission system. Energies 10, 977.

Pérez, T., Fossen, T., 2008. Time-vs. frequency-domain identification of parametric radiation force models for marine structures at zero speed. Model. Identif. Control 29, 1–19.

Polinder, H., 2013. Principles of electrical design of permanent magnet generators for direct drive renewable energy systems. In: Electrical Drives for Direct Drive Renewable Energy Systems. Woodhead Publishing Limited, pp. 30–50.

Polinder, H., Damen, M.E.C., Gardner, F., 2004. Linear PM generator system for wave energy conversion in the AWS. IEEE Trans. Energy Convers. 19, 583–589.

Polinder, H., van der Pijl, F.F.A., de Vilder, G.-J., Tavner, P.J., 2006. Comparison of direct-drive and geared generator concepts for wind turbines. IEEE Trans. Energy Convers. 21, 725–733.

Prado, M., Polinder, H., 2013. Case study of the Archimedes Wave Swing (AWS) direct drive wave energy pilot plant. In: Electrical Drives for Direct Drive Renewable Energy Systems. Woodhead Publishing Limited, pp. 195–218.

Qiu, S.-q., Ye, J.-w., Wang, D.-j., Liang, F.-l., 2013. Experimental study on a pendulum wave energy converter. China Ocean Eng. 27, 359–368.

Roberts, O., Jeffrey, H., MacGillivray, A., Guanche, R., de Andres, A., 2016. Beyond LCOE: A study of ocean energy technology development and deployment attractiveness. Sustain. Energy Technol. Assess. 19, 1–16.

Saenz-Aguirre, A., Ulazia, A., Ibarra-Berastegui, G., Saenz, J., 2021. Extension and improvement of synchronous linear generator based point absorber operation in high wave excitation scenarios. Ocean Eng. 239, 109844.

Stallard, T.J., Weller, S.D., Stansby, P.K., 2009. Limiting heave response of a wave energy device by draft adjustment with upper surface immersion. Appl. Ocean Res. 31, 282–289.

Suchithra, R., Ezhilsabareesh, K., Samad, A., 2019. Development of a reduced order wave to wire model of an OWC wave energy converter for control system analysis. Ocean Eng. 172, 614–628.

Tai, V.C., See, P.C., Merle, S., Molinas, M., 2012. Sizing and control of the electric power take off for a buoy type point absorber wave energy converter. Renew. Energy Power Qual. J. 1, 1614–1619.

Tan, J., Polinder, H., Laguna, A.J., Miedema, S., 2022a. A numerical study on the performance of the point absorber wave energy converter integrated with an adjustable draft system. Ocean Eng. 254, 111347.

Tan, J., Polinder, H., Laguna, A.J., Wellens, P., Miedema, S.A., 2021a. The influence of sizing of wave energy converters on the techno–economic performance. J. Mar. Sci. Eng. 9, 52.

Tan, J., Polinder, H., Wellens, P., Miedema, S., 2020. A feasibility study on downsizing of power take off system of wave energy converters. In: Developments in Renewable Energies Offshore: Proceedings of the 4th International Conference on Renewable Energies Offshore. RENEW 2020, CRC Press, Lisbon, Portugal, p. 140.

Tan, J., Wang, X., Jarquin Laguna, A., Polinder, H., Miedema, S., 2021b. The influence of linear permanent magnet generator sizing on the techno–economic performance of a wave energy converter. In: 2021 13th International Symposium on Linear Drives for Industry Applications. LDIA, pp. 1–6.

Tan, J., Wang, X., Polinder, H., Laguna, A.J., Miedema, S.A., 2022b. Downsizing the linear PM generator in wave energy conversion for improved economic feasibility. J. Mar. Sci. Eng. 10, 1316.

Tedeschi, E., Carraro, M., Molinas, M., Mattavelli, P., 2011. Effect of control strategies and power take-off efficiency on the power capture from sea waves. IEEE Trans. Energy Convers. 26, 1088–1098.

Tedeschi, E., Molinas, M., 2010. Impact of control strategies on the rating of electric power take off for wave energy conversion. In: IEEE International Symposium on Industrial Electronics. pp. 2406–2411.

Tedeschi, E., Molinas, M., 2012. Tunable control strategy for wave energy converters with limited power takeoff rating. IEEE Trans. Ind. Electron. 59, 3838–3846.

Temiz, I., Ekweoba, C., Thomas, S., Kramer, M., Savin, A., 2021. Wave absorber ballast optimization based on the analytical model for a pitching wave energy converter. Ocean Eng. 240, 109906.

Tokat, P., 2018. Performance Evaluation and Life Cycle Cost Analysis of the Electrical Generation Unit of a Wave Energy Converter. Chalmers Tekniska Hogskola (Sweden).

Wang, L., 2017. Modelling and Advanced Control of Fully Coupled Wave Energy Converters Subject to Constraints: the Wave-to-Wire Approach (Ph.D. thesis). Acta Universitatis Upsaliensis.

Wang, L., Hu, P., Chen, W., Feng, F., 2022a. Enhanced energy harvesting of wave energy converters in site-specific wave climates: A hybrid approach by geometric shape optimization and power take-off control. Ocean Eng. 257, 111553.

Wang, J., Hu, J., Pei, W., Yang, Z., Zhuang, J., Zhang, X., 2022b. In-depth design and multiobjective optimization of an integrated transformer for five-phase LLC resonant converters. IEEE Trans. Power Electron. 37, 13538–13553.

Wang, L., Li, H., Jiang, J., 2022c. A high-efficiency wave-powered marine observation buoy: Design, analysis, and experimental tests. Energy Convers. Manage. 270, 116154.

Wang, L., Lin, M., Tedeschi, E., Engström, J., Isberg, J., 2020. Improving electric power generation of a standalone wave energy converter via optimal electric load control. Energy 211, 118945.

Wang, J., Pei, W., Hu, J., Zhao, S., Zhuang, J., 2022d. Five-phase LLC resonant DC/DC converter utilizing CLC filter for current sharing. IEEE Trans. Ind. Electron..

Wang, L., Ringwood, J.V., 2021. Control-informed ballast and geometric optimisation of a three-body hinge-barge wave energy converter using two-layer optimisation. Renew. Energy 171, 1159–1170.

Wang, L., Zhao, T., Lin, M., Li, H., 2022e. Towards realistic power performance and techno–economic performance of wave power farms: The impact of control strategies and wave climates. Ocean Eng. 248, 110754.